Article:
Wells, J., Akram, M., Heeley, A. et al. (2026) Performance campaign of a chemical absorption pilot plant treating high CO2 content industrial process emissions. Carbon Capture Science & Technology, 20. 100659. ISSN: 2772-6568

https://doi.org/10.1016/j.ccst.2026.100659

20 (2026) 100659

Contents lists available at ScienceDirect

Carbon Capture Science & Technology

journal homepage: www.elsevier.com/locate/ccst

Full Length Article

Performance campaign of a chemical absorption pilot plant treating high CO_2 content industrial process emissions

Jack Wells [a,*], Muhammad Akram [a,b], Andy Heeley [b], Kevin J. Hughes [a], Derek B. Ingham [a], Mohamed Pourkashanian [a,b]

[a] School of Mechanical, Aerospace and Civil Engineering, Energy 2050, University of Sheffield, Sheffield, South Yorkshire, S3 7RD, United Kingdom
[b] Energy Innovation Centre, Sheffield Business Park, Europa Avenue South Yorkshire, Sheffield, S9 1ZA, United Kingdom

ARTICLE INFO

Keywords:
Decarbonisation
Chemical absorption
Process optimisation
Energy balance
Carbon capture
Heavy industry

ABSTRACT

Decarbonisation of critical hard-to-abate industrial sectors such as the iron and steel industry is crucial for meeting climate targets, with chemical absorption carbon capture identified as a key transitional technology. However, its application is hindered by a significant knowledge gap: the absence of publicly available and transparent performance benchmarks using conventional capture systems under elevated CO_2 conditions that are representative of industrial process emissions. An experimental performance campaign was conducted on the chemical absorption pilot plant at the Energy Innovation Centre (EIC) in Sheffield, UK. The study established a novel performance baseline across a wide operating envelope for flue gas concentrations ranging from 10 to 25 mol.% CO_2, achieving 90% capture efficiency using a 35 wt.% monoethanolamine (MEA) solvent. In addition, a methodology was developed to quantify solvent regeneration energy and its constituent components, complementing a system energy balance for each capture condition. The results provided experimentally validated insight into the relationship between operating conditions, capture performance, and energy demand at elevated CO_2 concentrations. The dataset established a robust baseline for conventional packed-bed systems and improved understanding of regeneration energy contributions under industrially relevant conditions. These findings are scalable for application to the design, operation and optimisation of chemical absorption systems in heavy industries and provide a reliable benchmark for future work on advanced solvents, process intensification and scale-up to commercial deployment.

1. Introduction

Anthropogenic greenhouse gas emissions in the post-industrial era are widely recognised as the primary driver of contemporary climate change (Intergovernmental Panel On Climate Change (IPCC), 2023). Atmospheric CO_2 concentrations have continued to rise, exceeding 430 ppm in 2026 (Lan et al., 2023), prompting increasingly ambitious decarbonisation targets across both national policies and international agreements (UNFCCC, 1992; Grubb, 2004; United Nations (UN), 2015; GOV.UK, 2019). Achieving these targets presents sector-specific challenges, particularly for industries where CO_2 emissions are intrinsically linked to core production processes (Climate Change Committee, 2025). Among these, the cement, petrochemical, and steel industries are notably referred to as hard-to-abate sectors (UNFCCC, 2024). The steel industry alone contributes approximately 2.6 Gt CO_2e annually, accounting for 7–9% of global anthropogenic emissions (Kim et al., 2022). With demand for crude steel expected to grow in the coming years (World Steel Association, 2026), mitigating these emissions must form an essential part of any industrial decarbonisation strategy (Swalec, 2021).

This substantial carbon footprint is primarily driven by the dominance of the blast furnace-basic oxygen furnace (BF-BOF) production

Abbreviations: ACP, amine capture plant; BF-BOF, blast furnace-basic oxygen furnace; CCS, carbon capture and storage; CDT, centre for doctoral training; CREDS, centre for research into energy demand solutions; DCC, developed carbon capture; DESNZ, department for energy security and next zero; EIC, energy innovation centre; EPSRC, engineering and physical sciences research council; ERDF, European regional development fund; HSS, heat stable salts; IFRF, international flame research foundation; L/G, liquid to gas; MEA, monoethanolamine; PB, packed-bed; PHW, pressurised hot water; RDFES, resilient decarbonised fuel energy systems; RPB, rotating packed bed; RTD, resistance temperature detectors; SRD, specific reboiler duty; SSG, specific steam generation.

* Corresponding author.
E-mail address: jackwellsuk@aol.com (J. Wells).

https://doi.org/10.1016/j.ccst.2026.100659
Received 28 May 2026; Received in revised form 29 June 2026; Accepted 10 July 2026
Available online 10 July 2026

route, which represented over 70% of global steel production in 2024 (World Steel Association, 2025). In this process, coke is used both as a reducing agent and as a fuel, resulting in inherently unavoidable CO_2 emissions. The blast furnace is the largest single emission source within this route, contributing approximately 70% of site-level CO_2 emissions (Wiley et al., 2011), with flue gas CO_2 concentrations upwards of 25 mol.% (Ren et al., 2025). Given the long operational lifetimes of blast furnaces (Nakano et al., 2020; Vogl et al., 2021), short-term decarbonisation strategies must focus on mitigating emissions from existing furnaces. In this context, carbon capture and storage (CCS) has been identified by the International Energy Agency as a key strategy to significantly reduce steel industry emissions (IEA, 2020a, 2020b, 2021).

Among post-combustion capture technologies, chemical absorption is well suited to treating steelmaking emissions (Ramírez-Santos et al., 2018), owing to the characteristic pressures and CO_2 concentrations of the flue gases (Han et al., 2014). As a mature and widely studied technology (Gruenewald and Radnjanski, 2016), it provides a robust and well-understood basis for industrial deployment. Monoethanolamine (MEA) is commonly adopted as the standard solvent for evaluating process behaviour and benchmarking alternative solvents and process configurations. However, despite extensive research into chemical absorption, studies have predominantly focused on flue gas compositions with low CO_2 concentrations, targeting process emissions from power generation (Biermann et al., 2022). In their comprehensive review of pilot-scale campaigns, Biermann et al. (2022) highlighted the absence of MEA-based pilot data for CO_2 concentrations above 15 mol.% . In the same study, they partially addressed this knowledge gap through pilot-scale testing at 18–20 mol.% CO_2 using 30 wt.% MEA, achieving 90% capture efficiency with a minimum specific reboiler duty (SRD) of 3.7 MJ/kg•CO_2. While this represents a significant advancement, it remains below CO_2 concentrations characteristic of blast furnace emissions, indicating that further investigation at higher concentrations is required.

Other pilot-scale studies reinforce this limitation. Notz et al. (2012) conducted a comprehensive experimental campaign using 30 wt.% MEA, but were limited to a maximum CO_2 concentration of 13.4 mol.%, where they achieved a capture efficiency of only 43.67%. Similarly, studies by Krótki et al. (2023), Kwak et al. (2012), and Knudsen et al. (2009) achieved 90% capture efficiency using MEA, but at CO_2 concentrations ranging from 12 to 15 mol.%. Across these studies, variations in plant design, operating conditions, and process configurations introduce significant differences in reported performance metrics, making direct comparison challenging. Nevertheless, they collectively demonstrate that pilot-scale validation at elevated CO_2 concentrations remains limited.

In parallel with the development of pilot-scale datasets for benchmarking purposes, significant research effort has been directed towards reducing the energy penalty associated with chemical absorption carbon capture. Process intensification strategies have been proposed to address this challenge, including improvements to solvent regeneration through catalytic or enhanced desorption approaches (Zhao et al., 2026), as well as alternative gas-liquid contacting configurations such as rotating packed beds (RPBs) (Akram et al., 2025a), membrane-based contactors (Chen et al., 2020), and many other advanced process configurations discussed in the wider literature (Oyenekan and Rochelle, 2007; Le Moullec and Kanniche, 2011; Le Moullec et al., 2014). These approaches aim to reduce regeneration energy demand, improve mass transfer efficiency, and enhance overall process performance, with their performance ultimately assessed relative to benchmark data generated from conventional packed-column systems.

Consequently, there is a critical lack of experimentally validated performance data for MEA-based chemical absorption treating process emissions typical of the steel industry and other hard-to-abate sectors. Addressing this research gap is necessary to establish reliable performance benchmarks and inform process optimisation under elevated CO_2 concentrations.

The Energy Innovation Centre (EIC) in Sheffield houses a pilot-scale amine capture plant (ACP) capable of capturing up to one tonne of CO_2 per day. Previous studies on the ACP have primarily focused on flue gas concentrations up to approximately 10 mol.% (Akram et al., 2016, 2020; Aliyu et al., 2021). However, recent modelling work using the Developed Carbon Capture (DCC) model (Wells et al., 2025) predicted that the plant could achieve capture efficiencies of 90% or higher at significantly elevated CO_2 concentrations. These predictions motivated an experimental campaign investigating performance across a wide operating envelope, including comparisons between conventional packed-bed (PB) and RPB absorber configurations (Akram et al., 2025a).

The present study expands upon this work by focusing on the PB absorber and extending the experimental dataset to include flue gas CO_2 concentrations of 25 mol.%. In addition, a detailed energy balance methodology is developed to quantify solvent regeneration energy and its constituent components.

The objective of this study is to evaluate capture performance across a range of conditions representative of steel industry emissions, thereby establishing a novel pilot-scale dataset for MEA-based carbon capture at elevated CO_2 concentrations. This provides a robust baseline for future process optimisation and facilitates improved understanding of energy requirements in industrial carbon capture systems.

Experimental conditions were guided by DCC model predictions (Wells et al., 2025), with tests conducted at CO_2 concentrations of 25, 20, 15, and 10 mol.% at a fixed flue gas flow rate of 150 Nm^3/h. A capture efficiency of 90% was targeted for all capture conditions using a 35 wt.% MEA solvent.

2. Pilot plant technical specifications

The pilot-scale ACP at EIC is based on a conventional PB system. It is equipped with two absorber columns arranged in series, a stripper column with a reboiler and reflux vessel, a cross-heat exchanger, and a water wash system. A simplified plant layout is presented in Fig. 1.

The plant is designed to scrub between 100 to 250 Nm^3/h of flue gas using solvent flowrates up to 1200 kg/h. For this performance campaign, a synthetic flue gas comprising air with CO_2 injection was used rather than real flue gas. The gas flow rate was maintained at 150 Nm^3/h, while the CO_2 partial pressure was varied across test conditions. The synthetic flue gas bypassed the desulphurisation system and was blown into the absorber using a booster fan.

The absorber consists of two identical columns, each containing two packed beds, 3 m high and 250 mm in diameter, filled with Flexipac 350X structured packing from Koch Glitsch. Bucket-type liquid distributors are located at the solvent inlets at the top of each column, with liquid redistributors located between the two packed beds in each column. Gas distributors are located at the gas inlet at the bottom of each column. For this study, the absorber columns were operated in series with counter-current flow, though parallel and single column flow configurations are also possible. The absorbers each contain 12 distributed resistance temperature detectors (RTDs) for temperature monitoring and operate at atmospheric pressure.

A Coriolis flow meter measures the mass flow of lean solvent, regulated by a variable speed drive pump. Lean solvent flows down the absorber and contacts the flue gas, absorbing CO_2 in an exothermic reaction and cleaning the flue gas. The cleaned flue gas passes through a water wash column, 7.5 m high and 300 mm in diameter filled with IMTP25 random packing from Koch Glitsch. The water wash removes entrained solvent droplets carried over by the flue gas, minimising contaminant emissions from the ACP.

The rich solvent leaving the absorber is also measured with a Coriolis meter. Its level in the sump is controlled using a separate pump to ensure steady state operation. The rich solvent is then preheated via a plate type cross-heat exchanger, using heat from the regenerated lean solvent returning from the reboiler. The preheated rich solvent enters the top of the stripper column, where it is heated further to a temperature between

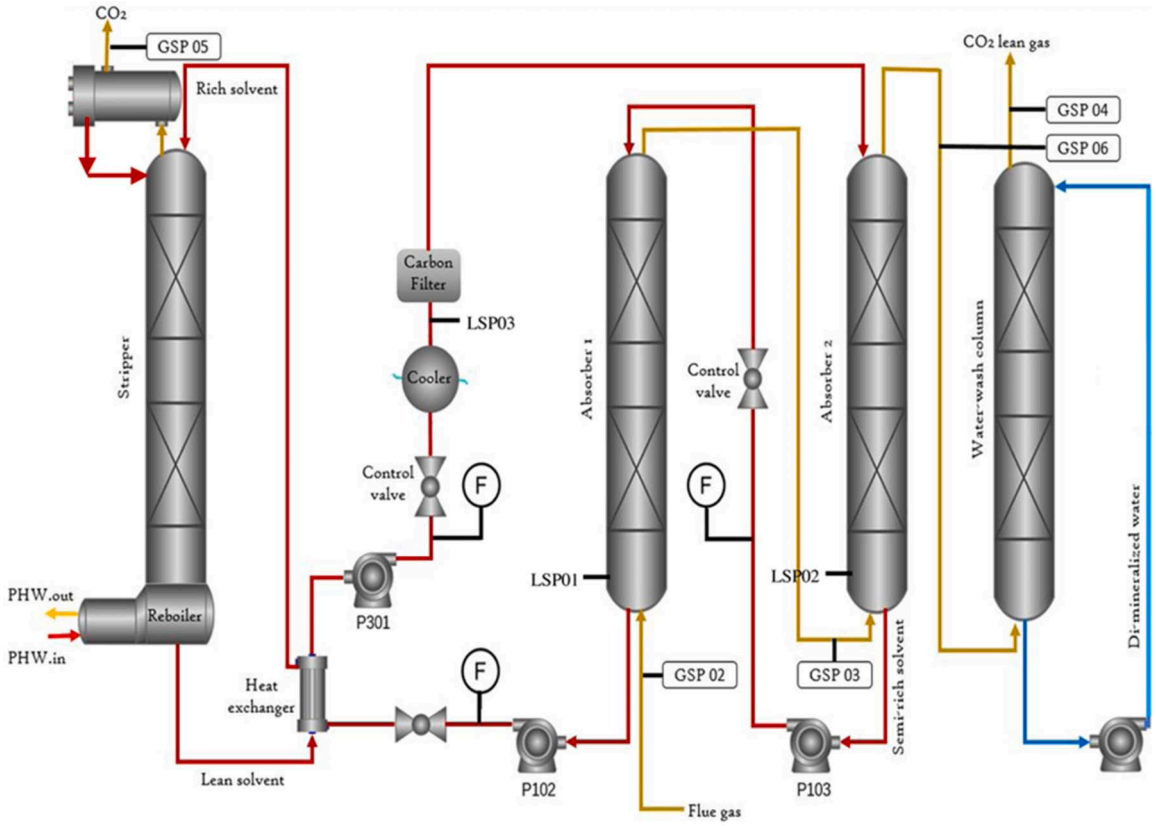

Fig. 1. Simplified flow diagram of the EIC ACP (Akram et al., 2021).

110 and 125°C, dependent on stripper pressure. In this campaign the pressure was maintained at 1.2 bara. The elevated temperature reverses the absorption process in an endothermic reaction, releasing the captured CO_2 and regenerating the solvent. Like the water wash, the stripper column is also 7.5 m high and 300 mm in diameter, packed with IMTP25 random packing. The stripper contains 9 distributed RTDs for temperature monitoring.

Solvent regeneration is driven by steam generation in the reboiler, which is supplied with pressurised hot water (PHW) maintained at a pressure between 4.8 and 5.0 bara. Changes in PHW flow rate or temperature directly influence solvent regeneration. For this campaign, the PHW flow rate was maintained between 11,750 and 11,800 L/h with the incoming temperature varied between 112 and 121°C to achieve a capture efficiency of 90% for each capture condition.

The liberated CO_2 in the stripper overhead stream passes through an air cooler and reflux condenser. Pure CO_2 is vented through the top of the reflux vessel while condensed water and solvent are returned to the top of the stripper.

Regenerated hot lean solvent from the reboiler sump first passes through the cross-heat exchanger to preheat the incoming rich solvent before then passing through an air cooler. After cooling, the lean solvent passes through a carbon filter filled with acid-washed activated carbon to remove solvent degradation products before re-entering the absorber, completing the cycle. The water wash levels are replenished with demineralised water as needed, and solvent concentration is maintained through periodic addition of fresh solvent (Akram et al., 2016, 2020, 2025b; Rezazadeh et al., 2016; The University of Sheffield, 2023, 2024).

A summary of the technical specifications and operating parameter ranges for the EIC ACP are presented in Table 1 and Table 2, respectively.

Table 1
Technical specifications of the EIC ACP.

Equipment	Specification
Absorber Column	Two 250 mm diameter columns, providing up to 12 m total packed height Packing: 4 × 3 m packed beds of Flexipac 350X structured packing 12 RTDs in each column for temperature monitoring
Stripper Column	Single column of 300 mm diameter with 8 m total height Packing: IMTP25 random packing 9 RTDs for temperature monitoring
Cross-Heat Exchanger	Plate heat exchanger Maximum heat duty up to 43 kW
Stripper Reboiler	Supplied with pressurised hot water Electric boiler heat duty up to 72 kW

Table 2
Operating parameter ranges of the EIC ACP.

Parameter	Operational Range
Solvent Mass Flow Rate (CO_2 Free Basis)	300–1200 kg/h
Flue Gas Volumetric Flow Rate	100–250 Nm^3/h
Stripper Column Pressure	1.0–3.0 bara

3. Methodology

The following key measurements were recorded during the testing period:

- Temperature, flow and pressure readings were taken at various locations across the ACP.
- Flue gas compositions were measured using a Gasmet FTIR analyser.
- Solvent samples were analysed using a Mettler Toledo auto-titrator.

These three sets of measurements were then used to calculate key performance indicators for each capture condition, including specific reboiler duty (SRD), CO_2 capture efficiency, liquid to gas (L/G) ratio, solvent/CO_2 ratio, solvent concentrations, and solvent CO_2 loadings. The L/G ratio used in this study refers exclusively to the absorber operating condition and is defined as the mass flow rate of lean solvent relative to the mass flow rate of flue gas, providing a consistent descriptor of the operating condition of the integrated absorber-stripper system at steady state. The accompanying solvent/CO_2 ratio is defined as the mass flow rate of pure (CO_2-free) solvent relative to the mass flow rate of CO_2 in the flue gas and is presented as an additional normalised performance metric for comparing operating conditions.

3.1. Flue gas and solvent analysis

Flue gas analysis on the EIC ACP was performed using a Gasmet DX4000 FTIR analyser. Flue gas samples were extracted from different locations on the ACP using isokinetic sampling probes and delivered to the FTIR via heated filters, heated sampling lines, and a heated cabinet containing solenoid valves for switching between sampling points. The entire sampling system was maintained at 180°C to prevent condensation. The analyser averaged data over 15 second sampling intervals.

The CO_2 capture efficiency was calculated around the absorber using Method 3 as described by Thimsen et al. (2014). This method requires determination of the CO_2 mass flow rates in the inlet and outlet flue gas streams, denoted in Fig. 1 as GSP02 and GSP04, respectively. Real-time monitoring of flue gas composition enabled identification of steady state conditions, defined by a stable outlet composition. Steady state conditions were maintained for approximately one hour, with data averaged over this interval. FTIR measurements and process data were combined to determine the mass flow rates of the gas streams and their individual components. Accordingly, the capture efficiency for a given capture condition can be determined by calculating the percentage difference between the mass of captured CO_2 and the CO_2 mass flow at the absorber inlet:

$$\eta_{\text{capture}} = \frac{\dot{m}_{CO_2,\ \text{in}} - \dot{m}_{CO_2,\text{out}}}{\dot{m}_{CO_2,\ \text{in}}} \cdot 100 \quad (1)$$

Where:

$\dot{m}_{CO_2,\ \text{in}}$ = mass flow rate of CO_2 entering the absorber (kg/h)
$\dot{m}_{CO_2,\text{out}}$ = mass flow rate of CO_2 exiting the absorber (kg/h)
η_{capture} = CO_2 capture efficiency (%)

At the end of a steady state period, solvent analyses were performed using a T9 Mettler Toledo auto-titrator to determine the concentration and CO_2 loading of each sample. Lean samples were taken at LSP03 in Fig. 1, and rich samples were taken at LSP01. Chemical titrations were conducted in "semi-automatic" mode, where sample preparation and mass measurements were done manually. Results were recorded using LabX software. The solvent concentration values consider the mass of CO_2 in the solvent in its calculation in addition to the MEA and H_2O.

3.2. Heat duty calculations

The reboiler duty is determined using measurements from the PHW circuit. As the flow rate and pressure of the PHW is held constant during testing, the amount of heat transferred to the solvent in the reboiler is directly proportional to the temperature difference between the inlet and outlet PHW streams:

$$Q_{\text{reboiler}} = \dot{m}_{\text{PHW}} \cdot C_{p,\text{PHW}} \cdot \Delta T_{\text{PHW}} \quad (2)$$

Where:

Q_{reboiler} = reboiler heat duty (kJ/h)
$\dot{m}_{\text{PHW}}$ = mass flow rate of the PHW (kg/h)
$C_{p,\text{PHW}}$ = specific heat capacity of the PHW (kJ/(kg·K))
ΔT_{PHW} = temperature difference between the inlet and outlet PHW streams (°C)

The specific reboiler duty is defined as the amount of energy required by the reboiler to release a unit mass of CO_2, calculated by dividing the total energy input by the mass of CO_2 captured:

$$q_{\text{reboiler}} = \frac{Q_{\text{reboiler}}}{\dot{m}_{CO_2,\ \text{in}} - \dot{m}_{CO_2,\text{out}}} \quad (3)$$

Where:

q_{reboiler} = specific reboiler duty (MJ/(kg•CO_2))

3.3. Column temperature profiles

While a comprehensive assessment of column performance requires detailed knowledge of liquid and gas phase composition profiles along the packing height (Weiland et al., 2015), including local mass transfer rates and resistances, obtaining such data during plant operation is often impractical. Composition analysis typically requires complex, slow, and expensive instrumentation that is not suited for continuous operational feedback. Temperature profiles, by contrast, offer a simple, robust, and continuous alternative for process monitoring, providing real-time insight into the underlying heat and mass transfer processes occurring within the columns.

The utility of temperature profiles arises from the strong relationship between heat generation/consumption and CO_2 mass transfer. Absorption of CO_2 into MEA is an exothermic process, while solvent regeneration within the stripper is endothermic. Consequently, local temperature variations provide an indication of the location and relative intensity of mass transfer activity within the columns. They can therefore be used to identify characteristic operating regimes, diagnose process limitations, and assess overall column performance during operation (Hatcher et al., 2013; Weiland et al., 2015; Gibbins, 2023). Detailed descriptions of these regimes and their interpretation have been discussed previously by Wells et al. (2025) and are therefore not repeated here.

4. Primary experimental results

4.1. Experimental design

For this performance campaign, a synthetic flue gas with a fixed flow rate of 150 Nm^3/h was used with four different CO_2 concentrations investigated: 25, 20, 15, and 10 mol.%. Solvent flow rate was varied in 100 kg/h increments according to predictions made by the DCC model (Wells et al., 2025), with the reboiler duty adjusted to achieve 90% capture efficiency for each condition. The stripper pressure was fixed at 1.2 bara.

A solvent concentration of 35 wt.% MEA was selected based on prior DCC model predictions, which indicated that operation at the elevated CO_2 concentrations investigated could be achieved with lower solvent circulation rates while remaining within the operating limits of the ACP. This selection is consistent with previous studies demonstrating that increasing MEA concentration from 30 to 40 wt.% can reduce solvent circulation requirements and regeneration energy, albeit with increased solvent degradation and corrosion potential (Brigman et al., 2014; Akram et al., 2020).

Chemistry data was unavailable for a subset of operating conditions; these were excluded from the final dataset. The conditions retained for analysis are presented in Table 3.

During analysis, the inlet and outlet temperatures of the cross-heat exchanger were found to be consistently underestimated due to

Table 3
Experimental matrix of solvent flow rates and CO_2 concentrations in gas flows of 150 Nm^3/h.

Solvent Flow kg/h	CO_2 Concentration			
	25 mol.%	20 mol.%	15 mol.%	10 mol.%
1200		✓		
1100	✓	✓		
1000	✓	✓		
900	✓	✓		
800	✓	✓	✓	
700			✓	✓
600			✓	
500				✓
400				✓
300				✓

inadequate insulation of the RTDs, which exposed part of the sensors to ambient conditions. As a result, these measurements were deemed unreliable and omitted from the analysis. Although not crucial to the primary results, their exclusion prevents accurate determination of the cross-heat exchanger duty and approach temperature between the hot rich and hot lean solvent streams. This limitation is addressed and accounted for in the system energy balance that follows the primary results. Improved RTD installation or replacement of the affected sensors will permit direct evaluation of heat exchanger performance in future campaigns.

Throughout this study, capture conditions are labelled using a two-part naming convention: the first number indicates the flue gas CO_2 concentration in mol.%, and the second number represents the solvent flow rate in kg/h. For example, condition 25_1100 corresponds to a CO_2 concentration of 25 mol.% treated with 1100 kg/h solvent. The primary results of the performance campaign are presented in Table 4.

The detailed analysis of the 25 mol.% CO_2 conditions is presented in Section 4.2, while the remaining analyses of the 20, 15, and 10 mol.% CO_2 conditions are detailed in Appendix (A). In addition, a statistical uncertainty analysis following a 1σ framework was applied across the presented results, with the methodology and calculated uncertainties for the primary experimental data presented and discussed in the Supplementary Materials.

4.2. 25% CO_2 flue gas capture conditions

Key performance metrics for conditions with a flue gas CO_2 concentration of 25 mol.% are shown in Fig. 2.

The tested range of solvent flow rates successfully captured the approximate location of the optimal L/G ratio, as indicated by the minimum observed SRD of 3.83 MJ/kg•CO_2 at a solvent flow of 900 kg/h in Fig. 2A, corresponding to an L/G ratio of 4.01 for a lean solvent concentration of 32.26 wt.% MEA. The existence of an optimal solvent flow rate reflects the energy trade-off between solvent circulation rate and the degree of solvent regeneration required to achieve the target capture efficiency. At lower solvent flow rates, a greater solvent cyclic capacity is required to achieve the desired CO_2 capture rate, necessitating deeper solvent regeneration within the stripper and increasing the energy demand associated with solvent regeneration. Conversely, at higher solvent flow rates, the cyclic capacity is reduced, but a larger mass of solvent must be heated and circulated through the process, increasing the thermal duty associated with solvent regeneration.

The minimum SRD therefore occurs at the point where these competing effects are balanced. Within the tested operating range, this balance was observed at a solvent flow rate of approximately 900 kg/h. While the experimental resolution does not permit identification of a precise optimum, the similar SRD values observed at 800 and 1000 kg/h indicate that the optimal operating region lies close to 900 kg/h.

Notably, only the 900 kg/h condition achieved the target capture

Table 4
Primary experimental results for the performance campaign across a range of flue gas CO_2 concentrations and solvent flow rates.

Parameter	Units	Capture Conditions														
		25_800	25_900	25_1000	25_1100	20_800	20_900	20_1000	20_1100	20_1200	15_600	15_700	15_800	10_300	10_400	10_500	10_700
Flue Gas CO_2 Concentration	mol.%	24.24	24.99	24.99	24.99	20.18	20.18	20.11	20.11	20.07	15.14	15.00	15.04	10.15	10.01	10.03	10.01
Solvent Mass Flow Rate	kg/h	800	900	1000	1100	800	900	1000	1100	1200	600	700	800	300	400	500	700
Flue Gas Volumetric Flow Rate	Nm^3/h	153	153	152	152	151	151	151	152	153	152	151	151	149	147	149	149
Flue Gas Mass Flow Rate	kg/h	223.36	224.32	223.47	223.70	216.87	217.45	217.63	218.15	219.30	213.32	212.55	211.41	204.01	202.28	204.73	204.72
Flue Gas CO_2 Mass Flow Rate	kg/h	72.66	74.99	74.71	74.78	59.78	59.94	59.78	59.92	60.18	45.18	44.62	44.49	29.64	28.99	29.40	29.34
Liquid to Gas Ratio	kg/kg	3.58	4.01	4.47	4.92	3.69	4.14	4.59	5.04	5.47	2.81	3.29	3.78	1.47	1.98	2.44	3.42
Solvent to CO_2 Ratio	kg/kg	10.44	11.24	12.53	13.69	12.51	13.97	15.49	16.95	18.35	12.44	14.60	16.64	9.79	13.16	15.90	22.16
Flue Gas Temperature	°C	11.7	12.1	11.1	11.4	8.9	9.4	9.9	10.8	12.5	12.4	11.0	9.2	6.2	3.8	7.9	7.2
Lean Solvent Temperature	°C	33.9	37.1	37.3	38.1	30.3	31.1	33.5	35.9	37.4	28.2	30.3	31.9	28.7	29.5	35.2	36.6
Lean Solvent Concentration	wt.%	32.92	32.26	32.08	32.00	33.42	33.09	32.99	32.95	33.03	33.05	32.93	32.67	31.52	29.23	30.67	28.47
Rich Solvent Concentration	wt.%	30.05	30.59	30.52	30.42	31.43	31.20	31.43	31.74	31.36	31.49	31.20	31.67	30.66	27.32	29.37	27.47
Lean Solvent Loading	mol/mol	0.219	0.274	0.276	0.301	0.270	0.291	0.312	0.324	0.335	0.265	0.291	0.318	0.146	0.220	0.294	0.347
Rich Solvent Loading	mol/mol	0.542	0.545	0.539	0.521	0.517	0.521	0.533	0.504	0.508	0.539	0.531	0.533	0.504	0.544	0.535	0.539
Solvent Capacity	mol/mol	0.323	0.271	0.263	0.220	0.247	0.230	0.221	0.180	0.173	0.274	0.240	0.215	0.358	0.324	0.241	0.192
Absorber Bottom Temperature	°C	37.6	45.5	45.7	47.86	45.7	43.3	48.0	53.4	52.4	39.4	46.6	47.6	16.1	22.7	36.9	40.8
Stripper Top Temperature	°C	73.2	75.8	75.8	76.4	74.7	73.3	75.3	78.9	78.7	74.5	77.3	78.4	99.0	75.6	75.6	76.5
Stripper Bottom Temperature	°C	112.0	111.7	110.9	110.1	110.57	110.1	109.3	108.9	108.3	110.9	111.3	110.2	111.4	110.7	110.3	108.3
Stripper Reboiler Heat Duty	kW	70.96	72.42	71.60	72.30	58.54	62.00	63.63	63.13	65.14	42.97	45.15	47.53	51.97	30.96	30.24	35.48
Specific Reboiler Duty	MJ/kg•CO_2	4.05	3.83	4.04	4.14	3.86	4.12	4.22	4.24	4.37	3.79	4.05	4.21	7.15	4.29	4.13	4.83
CO_2 Capture Efficiency	%	86.73	90.88	85.35	84.12	91.39	90.45	90.79	89.43	89.09	90.26	90.02	91.37	88.26	89.57	89.66	90.18

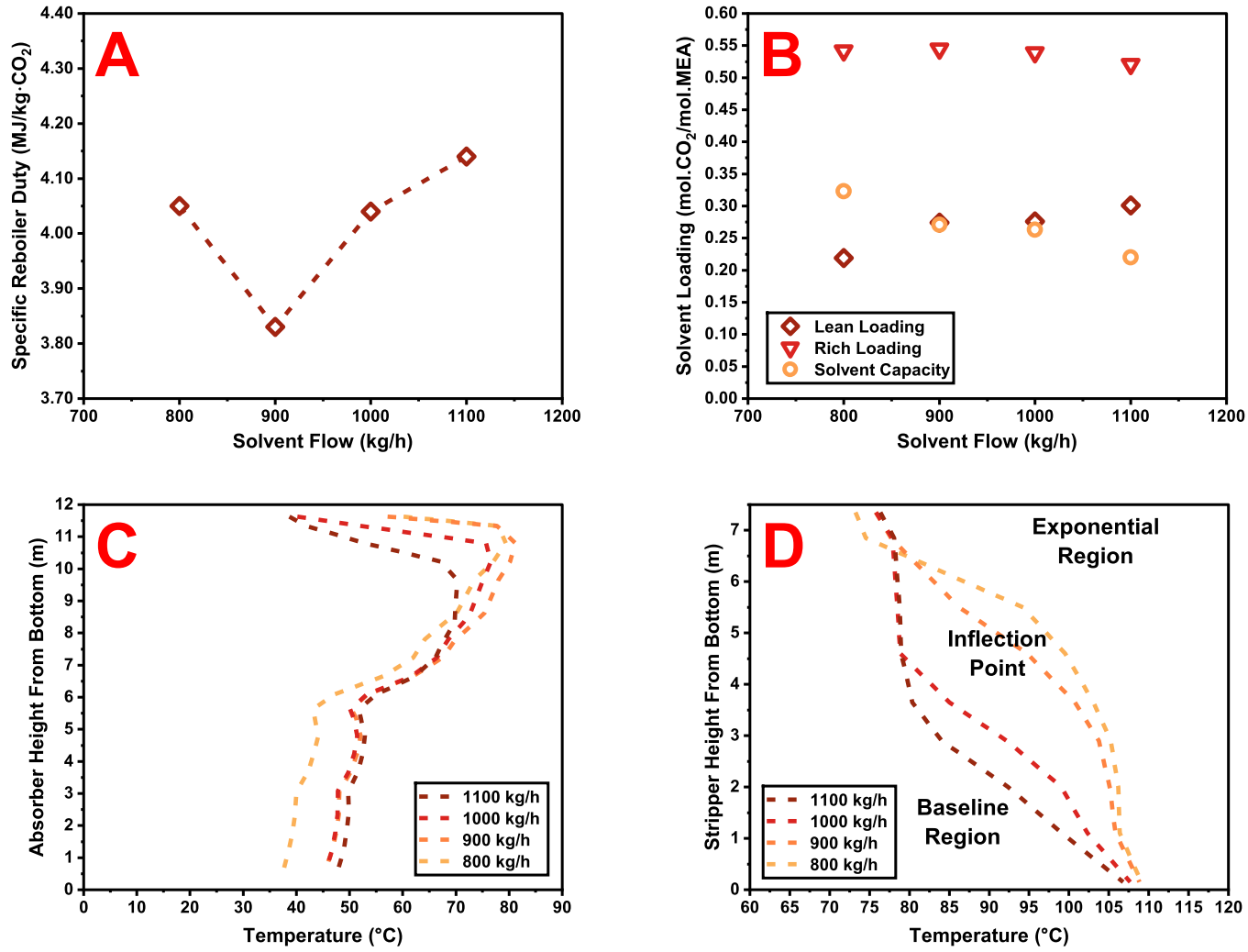

Fig. 2. Key performance metrics for solvent flow rates treating 150 Nm^3/h flue gas containing 25 mol.% CO_2, targeting 90% capture efficiency: (A) specific reboiler duty, (B) solvent loadings and capacity, (C) absorber temperature profiles, and (D) stripper temperature profiles.

efficiency, reaching 90.88%, while the remaining conditions achieved approximately 85% capture efficiency. The reboiler was operating at its maximum heat input for all cases, with the cross-heat exchanger assumed to be operating at maximum capacity. Consequently, the available thermal energy was only sufficient to achieve the target capture efficiency at the near-optimal solvent flow rate. At higher solvent flow rates, the reboiler duty was insufficient to adequately regenerate the increased solvent mass, whereas at lower solvent rates the deeper regeneration requirement resulted in a greater energy demand.

The analysis of solvent loadings in Fig. 2B shows that rich solvent loadings remain high and relatively constant across the tested range. A slight decrease is observed with increasing solvent flow, from 0.542 to 0.521. Values exceeding 0.5 suggest some physical dissolution of CO_2 into the MEA, indicating that once chemical absorption is maximised, the extent of physical dissolution is influenced by solvent residence time in the absorber.

In contrast, lean loading increases with solvent flow, rising from 0.219 to 0.301 as flow increases from 800 to 1100 kg/h. Solvent regeneration depth reduces with increasing flow rate as less solvent cyclic capacity is required to achieve the target capture efficiency. The lean loading at 900 kg/h is notably higher than expected, approaching that at 1000 kg/h, suggesting a possible measurement error associated with sampling and titration procedure. Based on the trend in Fig. 2B, a value closer to 0.25 would be expected, consistent with predictions from the DCC model (Wells et al., 2025).

The absorber temperature profiles in Fig. 2C align with expected behaviour. As solvent flow increases, the profiles shift from a rich-pinched state towards a bulge-pinched profile, indicating that the driving force for CO_2 absorption moves lower in the column. This distributes the reaction zone and flattens the temperature peak. At absorber heights of 6 m and below, corresponding to absorber 1 in the series configuration, minimal temperature variation is observed across all flow conditions, suggesting that the majority of CO_2 absorption occurred in absorber 2 under the operating conditions investigated. The limited variation in absorber 1 is likely due to a combination of ambient heat losses and the thermal content of the downflowing solvent.

These observations suggest that the full absorber height was not fully utilised within the operational envelope explored in the present study, and that similar capture performance may have been achievable with a reduced absorber height. However, absorber utilisation is strongly dependent on operating conditions, including flue gas composition, solvent flow rate, and column hydrodynamics. Consequently, the present results should not be interpreted as evidence that absorber 1 would be unnecessary under a broader operational envelope. Further investigation comparing single-column, series, and parallel operation would be required to assess the performance implications of alternative absorber configurations.

The stripper temperature profiles in Fig. 2D illustrate the distinct operating regimes typical of a stripping column (Gibbins, 2023). High solvent flow rates correspond to baseline operation, while low flow rates

result in exponential operation. The transition between these two regions, known as the inflection point, is characterised by a smooth temperature increase from top to bottom and corresponds to the minimum SRD for a given condition. Based on Fig. 2D, the 900 kg/h condition closely approximates this point, consistent with the minimum SRD identified in Fig. 2A. At higher flow rates ≥1000 kg/h, the system enters the baseline region, increasing SRD due to the additional energy required to heat higher solvent flows. At lower flow rates ≤800 kg/h, operation shifts to the exponential region, increasing SRD because reduced solvent flow rates require deeper solvent regeneration, resulting in greater steam demand.

4.3. SRD and solvent loading analysis

With trends at individual CO_2 concentrations established, the results were collated to assess overall system performance and identify broader patterns for prediction and validation of expected behaviour. For clarity, the 10 mol.% CO_2 condition at 300 kg/h is excluded, as it represented an extreme and suboptimal operating point that obscured trends in the remaining data.

Fig. 3 presents the SRD and lean loading against L/G ratio for conditions targeting 90% capture efficiency.

Fig. 3A presents SRD as a function of L/G ratio across the different capture conditions. The 10 mol.% CO_2 condition exhibits a higher minimum SRD than the higher concentration conditions, with values of 4.13 and 3.83 MJ/kg•CO_2 for 10 and 25 mol.% CO_2, respectively. This 7.3% reduction reflects the improved thermodynamic efficiency of capturing CO_2 at higher concentrations. The minimum SRDs for the 10 and 25 mol.% conditions correspond closely to the stripper inflection point, indicating operation near the optimal L/G ratio. In contrast, the 15 and 20 mol.% conditions do not clearly reach this point, with SRD continuing to decrease at the lowest tested L/G ratios. As these conditions remain within the stripper baseline region, further reductions in L/G ratio would be expected to lower SRD below the minimum observed for 25 mol.% CO_2, representing a greater reduction in SRD over the 10 mol.% minimum. Overall, the results suggest that SRD initially decreases with increasing CO_2 concentration before rising again as system limits are approached. This behaviour is consistent with DCC model predictions (Wells et al., 2025), where increasing CO_2 concentration improves efficiency until constrained by heat integration limits of the cross-heat exchanger.

Fig. 3B presents the lean solvent loading as a function of the L/G ratio across the different capture conditions. In all cases, lean loading increases approximately linearly with L/G ratio, reflecting the relationship between solvent flow and loading for a fixed CO_2 capture target. A clear offset is observed between CO_2 concentrations: at a given L/G ratio, lean loading increases by approximately 0.05 between adjacent conditions, indicating greater solvent capacity requirements at higher CO_2 concentrations. Conversely, achieving the same lean loading requires progressively higher L/G ratios, differing by approximately 0.8 between adjacent trendlines. The 25 mol.% CO_2 point at L/G 4.01 deviates from this trend and is attributed to a measurement anomaly, as discussed previously.

Fig. 4 presents SRD as a function of lean loading and solvent capacity across the different capture conditions, enabling estimation of the corresponding solvent properties for a given SRD.

The dashed lines in Fig. 4 represent partial trendlines derived from experimental data and adjusted to reflect ideal operating behaviour. In Fig. 4A, points to the right of the minimum correspond primarily to baseline operation, while those to the left reflect the exponential region; this relationship is reversed in Fig. 4B. Fig. 4A shows that, as solvent flow shifts towards the inflection point, SRD decreases to a minimum at an optimal lean loading of approximately 0.23. This suggests that optimal L/G ratios correspond to lean loadings near this value. The lowest SRD points for the 15 and 20 mol.% CO_2 conditions remain above this optimum, reinforcing that lower lean loadings and SRDs are achievable. The 25 mol.% CO_2 point appears shifted to higher lean loading due to measurement error, while the 10 mol.% CO_2 condition lies close to the trendline but at a higher SRD, consistent with its lower thermodynamic efficiency.

Fig. 4B presents SRD as a function of solvent capacity, accounting for variation in rich loading. The minimum in the trendline suggests an optimal solvent capacity of approximately 0.275. As with Fig. 4A, the 15 and 20 mol.% CO_2 conditions are expected to shift towards this optimum, while the corrected 25 mol.% CO_2 point would align more closely with the trend. The 10 mol.% CO_2 condition remains an outlier, with consistently higher SRD values.

Overall, the trendlines indicate a minimum achievable SRD of approximately 3.70 MJ/kg•CO_2 for 90% capture efficiency under the current operating configuration. This value aligns closely with the SRD values reported by Biermann et al. (2022), where an SRD range of 3.6–3.8 MJ/kg•CO_2, with an average of 3.70 MJ/kg•CO_2, was achieved at 90% capture efficiency for a flue gas CO_2 concentration of 20 mol.% using 30 wt.% MEA.

4.4. Solvent degradation considerations

Although solvent degradation was not investigated in the present

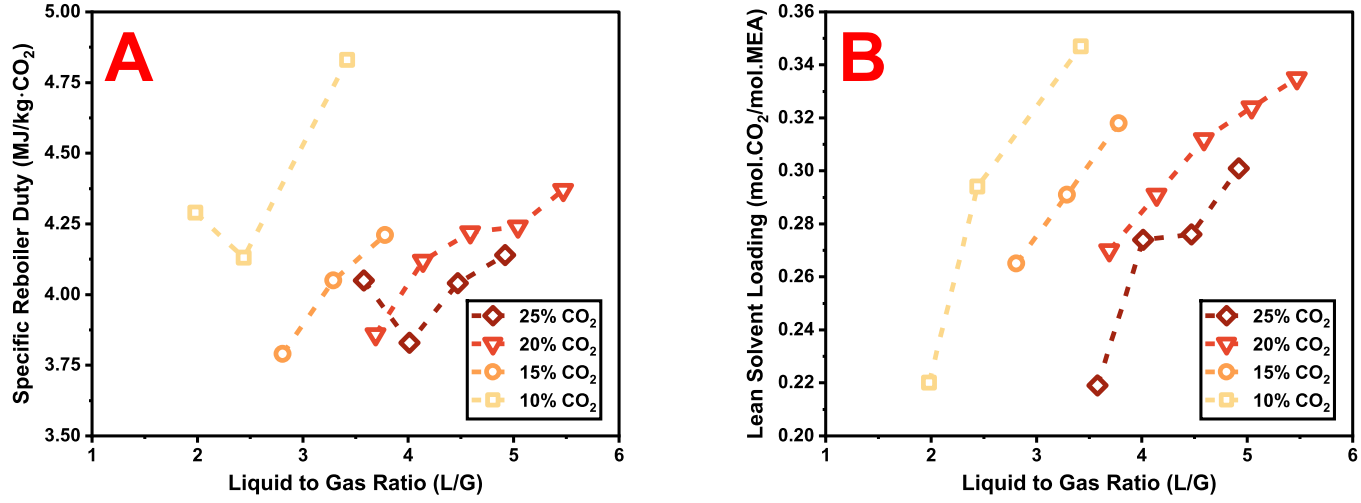

Fig. 3. (A) specific reboiler duty and (B) lean solvent loading, against liquid to gas ratio for solvent flow rates treating 150 Nm^3/h flue gas containing different CO_2 concentrations, targeting 90% capture efficiency.

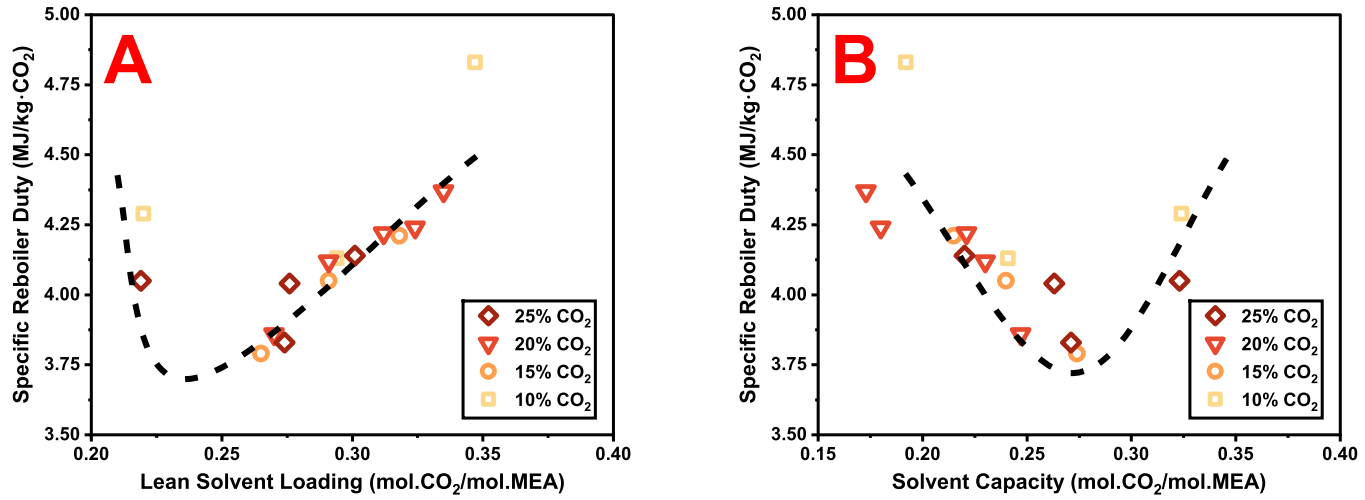

Fig. 4. Specific reboiler duty against: (A) lean solvent loading and (B) solvent capacity, for solvent flow rates treating 150 Nm^3/h flue gas containing different CO_2 concentrations, targeting 90% capture efficiency.

study, it remains an important consideration for long-term operation of MEA-based capture systems. Thermal degradation is typically associated with elevated temperatures within the stripper and reboiler, while oxidative degradation occurs predominantly within the absorber due to contact with oxygen present in the flue gas. Specific degradation products are highly dependent on process operating conditions. A review by Gouedard et al. (2012) discussed the main oxidative and thermal degradation products for MEA and other solvents, noting that detailed reaction mechanisms are incomplete for some products. The degradation of MEA has been shown to be dominated by oxidative degradation over thermal degradation in an industrial environment (Lepaumier et al., 2011; Salih et al., 2021), owing to typical process operation conditions. Thermal degradation is a slow process at typical operating temperatures (Zoannou et al., 2013), where the impact can be significantly reduced if the reboiler temperature is held below 110°C (Davis and Rochelle, 2009).

A major and detrimental consequence of both solvent degradation and the presence of flue gas impurities is the formation of corrosive heat stable salts (HSS), formed from the reaction of the basic alkanolamine with strong acids (Thompson et al., 2017). These acids can be introduced via the flue gas, such as SO_x, NO_x, and HCl, or generated in situ as byproducts from oxidative degradation, such as formic and acetic acid (Gouedard et al., 2012; Vega et al., 2014; Thompson et al., 2017). A key characteristic of HSS is their high thermal stability, they do not break down or decompose during solvent regeneration and therefore accumulate within the system (Verma and Verma, 2009).

The interactions between degradation, corrosion, and process performance are closely coupled. Both oxidative and thermal degradation pathways contribute to the formation of corrosive HSS. Corrosion of plant equipment releases metal ions into the solvent, which can catalyse further oxidative degradation and accelerate solvent deterioration. The accumulation of degradation products reduces the solvent's absorption capacity, requiring increased solvent circulation rates or solvent management strategies to maintain capture efficiency, thereby increasing regeneration energy demand and overall operating requirements.

Moser et al. (2020) documented this behaviour during an 18-month degradation campaign, where the solvent circulation rate was gradually increased from 4,000 to 6,000 kg/h to maintain 90% capture efficiency as degradation products accumulated. They noted how the degradation products increased in a non-linear fashion, demonstrating how a runaway degradation cycle can occur in capture systems. Two management strategies were employed to reduce degradation products: a solvent purge, where a portion of the contaminated solvent was removed and replaced with fresh solvent, and solvent reclamation by ion exchange. Neerup et al. (2023) investigated MEA degradation during approximately 2,000 hours of operation on a waste-to-energy plant, including assessment of solvent degradation products, emissions, and solvent management strategies. In addition to the experimental campaign, the authors compiled a comprehensive summary of degradation and emissions studies reported across capture facilities worldwide, encompassing conventional alkanolamine solvents as well as proprietary and novel alternatives. As such, the work provides a valuable reference for readers seeking a broader overview of long-term solvent degradation behaviour and mitigation strategies beyond the scope of the present study.

The present study was completed over a period of approximately two weeks using fresh solvent and synthetic flue gas, with the reboiler temperature held below 112°C. Consequently, solvent degradation is not expected to have materially influenced the reported capture efficiencies, solvent loadings, or SRD values. However, the long-term implications of operating with 35 wt.% MEA, including solvent degradation, corrosion, solvent reclaiming requirements, and associated operating costs, have not been evaluated and should be considered in future studies aimed at industrial implementation.

5. System energy balance

5.1. Introduction to the energy balance

Following analysis of the primary experimental data, an energy balance was constructed around the stripper for each capture condition. Stream energy contents and relevant process parameters were evaluated within the defined system boundaries, as illustrated in Fig. 5. Each stream is labelled by composition and assigned a unique identifier used consistently throughout the calculations.

The energy balance methodology follows that of Akram et al. (2016), with the following assumptions applied to ensure a consistent basis:

- Complete desorption of captured CO_2 in the reboiler.
- Steam generation occurs exclusively in the reboiler.
- MEA remains entirely in the liquid phase (no vaporisation).
- Gas and liquid streams are in thermal equilibrium at the bottom of the column.
- The stripper overhead stream is CO_2 saturated with water at the exit temperature.
- Latent heat from condensing steam is fully transferred to the rich solvent.
- Condenser condensate is pure water, with no CO_2 reabsorption.

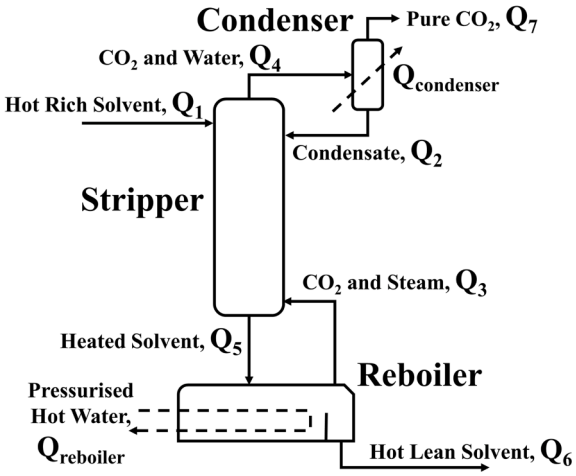

Fig. 5. Energy balance around the overall stripper system.

Additional assumptions were required due to limitations in the available process data:

- Rich solvent inlet temperature is equal to the stripper top temperature.
- The condenser removes 100% of the water from the stripper overhead stream.

This first assumption was adopted to represent the rich solvent inlet condition in the absence of reliable cross-heat exchanger temperature measurements, which were identified as a limitation of this study. The approach is supported by the observed stripper temperature profile behaviour and the sensitivity of column RTDs, as discussed in Appendix (A.3). The RTD located closest to the rich solvent inlet and condensate return was observed to respond to changes in liquid temperature and was therefore considered representative of the incoming rich solvent stream. The second assumption is required to achieve closure of the mass and energy balances around the stripper system. In practice, a small amount of water remains in the CO_2 product stream; however, this quantity is negligible, with a typical mass fraction of less than 0.01.

5.2. Calculation basis

The energy content of a specific stream or individual component is determined using:

$$\boldsymbol{Q} = \dot{\boldsymbol{m}} \cdot \boldsymbol{C}_{\mathbf{p}} \cdot \Delta \boldsymbol{T} \tag{4}$$

Where:

$\boldsymbol{Q}$ = energy flow of a specific stream/component (kJ/h)
$\dot{\boldsymbol{m}}$ = mass flow rate of a specific stream/component (kg/h)
$\boldsymbol{C}_{\mathbf{p}}$ = specific heat capacity of a specific stream/component (kJ/(kg·K))
$\Delta \boldsymbol{T}$ = temperature change of a specific stream/component (K)

Specific heat capacities were obtained using reference values for individual components (The Engineering Toolbox, 2005; Bell et al., 2014; AspenTech, 2026), or calculated using the rule of mixtures. All energy calculations have a reference temperature of 0°C, such that $\Delta \boldsymbol{T}$ corresponds to the stream temperature in°C.

5.3. Condenser duty calculations

To perform the overall energy balance around the stripper, the energy contributions of the condenser streams are first evaluated. The local system boundary applied to the condenser is shown in Fig. 6.

The inlet vapour (stream 4) is cooled in the condenser, where all water is assumed to exit as condensate (stream 2), while dry CO_2 exits the top (stream 7). The condenser duty is calculated from the difference between inlet and outlet stream energies:

$$\boldsymbol{Q}_{\mathbf{condenser}} = \boldsymbol{Q}_4 - \boldsymbol{Q}_2 - \boldsymbol{Q}_7 \tag{5}$$

Where:

$\boldsymbol{Q}_{\mathbf{condenser}}$ = condenser duty (kJ/h)

The mass flow rate of CO_2 in streams 4 and 7 is taken as equal to the captured CO_2, determined previously. The water content of stream 4 is determined assuming saturation at the corresponding temperature. The mole fraction of water is calculated from the saturation pressure:

$$\boldsymbol{x}_{\mathbf{H_2O}} = \frac{\boldsymbol{P}_{\mathbf{saturation}}}{\boldsymbol{P}_{\mathbf{reboiler}}} \tag{6}$$

Where:

$\boldsymbol{x}_{\mathbf{H_2O}}$ = mole fraction of water in the stream (mol/mol)
$\boldsymbol{P}_{\mathbf{saturation}}$ = saturation pressure at the corresponding temperature (kPa)
$\boldsymbol{P}_{\mathbf{reboiler}}$ = pressure of the reboiler (kPa)

This is converted to a mass fraction and used to determine the total mass flow rate of stream 4, from which the condensate flow rate (stream 2) is obtained by difference with stream 7. With all stream flow rates defined, Eq. (4) is used to evaluate the energy of each stream and determine the condenser duty.

5.4. Steam production calculations

The energy balance around the stripper column is defined by the boundary shown in Fig. 7. Hot rich solvent (stream 1) enters near the top of the column and flows downward, mixing with condensate from the condenser (stream 2) and internally generated condensate from steam supplied by the reboiler (stream 3). The heated solvent exits the column base to the reboiler (stream 5), while CO_2 and residual water leave the top of the column (stream 4).

The overall energy balance around the stripper is expressed as:

$$\boldsymbol{Q}_1 + \boldsymbol{Q}_2 + \boldsymbol{Q}_3 = \boldsymbol{Q}_4 + \boldsymbol{Q}_5 \tag{7}$$

From the condenser analysis, $\boldsymbol{Q}_2$ and $\boldsymbol{Q}_4$ are known, while $\boldsymbol{Q}_1$ is calculated using Eq. (4). The remaining terms, $\boldsymbol{Q}_3$ and $\boldsymbol{Q}_5$, depend on the rate of steam generation in the reboiler, which is not directly known. Steam generated in the reboiler enters the column (stream 3), condenses as it rises, and contributes to the liquid stream leaving the column base (stream 5), thereby linking the mass and energy balances of these streams. The overall mass balance is given by:

$$\dot{\boldsymbol{m}}_1 + \dot{\boldsymbol{m}}_2 + \dot{\boldsymbol{m}}_3 = \dot{\boldsymbol{m}}_4 + \dot{\boldsymbol{m}}_5 \tag{8}$$

The energy of stream 3 is evaluated as the sum of CO_2 and steam contributions at the reboiler temperature:

$$\boldsymbol{Q}_3 = \boldsymbol{Q}_{3,\mathbf{CO_2}} + \boldsymbol{Q}_{3,\mathbf{H_2O}} \tag{9}$$

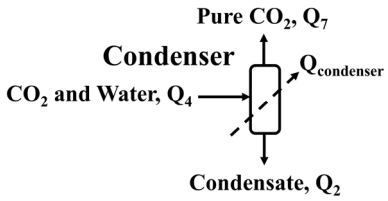

Fig. 6. Energy balance around the condenser.

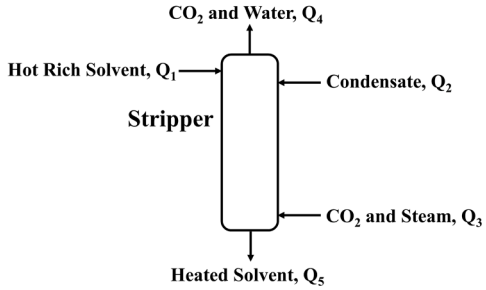

Fig. 7. Energy balance around the stripper column.

Q_{3,CO_2} is determined using Eq. (4), while Q_{3,H_2O} is determined using the following calculation:

$$Q_{3,H_2O} = Q_{steam} = \dot{m}_{steam} \cdot h_g \quad (10)$$

Where:

Q_{steam} = energy of flowing steam (kJ)
$\dot{m}_{steam}$ = mass flow rate of steam (kg/h)
h_g = specific enthalpy of saturated steam (kJ/kg)

Substitution into Eq. (7) allows the energy balance to be expressed as:

$$Q_1 + Q_2 + Q_{3,CO_2} + \dot{m}_{steam} \cdot h_g = Q_4 + Q_5 \quad (11)$$

Rearranging Eq. (11) allows the steam generation rate to be expressed as:

$$\dot{m}_{steam} = \frac{Q_4 + Q_5 - Q_1 - Q_2 - Q_{3,CO_2}}{h_g} \quad (12)$$

As Q_5 depends on the extent of steam condensation, an iterative approach is required to achieve closure of the mass and energy balances. The system is constrained by:

$$\dot{m}_{steam} = \dot{m}_5 - \dot{m}_1 = \dot{m}_3 - \dot{m}_7 \quad (13)$$

The solution is obtained by iterating the mass flow rate of stream 5 until the steam generation rate is consistent with both the difference between the solvent inlet and outlet flows, and the difference between vapour and CO_2 flows. This ensures that the amount of steam generated equals the net liquid accumulation within the system. The system of equations was solved using Microsoft Excel's Solver tool, with Eq. (11) subsequently verified to confirm consistency of the energy balance. At convergence, both mass and energy balances are satisfied within the system boundary shown in Fig. 7. The energy of the lean solvent leaving the reboiler was then evaluated using Eq. (4).

5.5. Additional calculations

The desorption energy was calculated indirectly from the overall stripper energy balance (Akram et al., 2016):

$$Q_{de} = Q_{reboiler} + Q_1 - Q_{condenser} - Q_6 - Q_7 \quad (14)$$

Where:

Q_{de} = desorption energy (kJ/h)

The specific steam generation (SSG) was determined as:

$$SSG = \frac{\dot{m}_{steam}}{\dot{m}_{CO_2,\ captured}} \quad (15)$$

Where:

SSG = specific steam generation (kg/kg)

The results of the stripper energy balance are presented in Table 5. Condition 10_300 was excluded due to non-physical results, where the calculated vapour flow exceeded that generated in the reboiler. Under deeply exponential conditions, a fraction of the generated steam does not fully condense within the column. As a result, the assumption of complete latent heat transfer to the solvent, and the corresponding saturation-based estimation of water content in the overhead stream, are no longer valid. Consequently, the energy balance is considered reliable only for conditions in which complete steam condensation occurs within the column, as indicated by stripper temperature profiles.

5.6. Energy balance discussion

The energy balance analysis reveals consistent trends across the evaluated terms. For the major energy contributions (Q_1, Q_3, Q_5, Q_6, and $Q_{reboiler}$), as well as steam generation and associated energy ($\dot{m}_{steam}$ and Q_{steam}), values generally increase with both flue gas CO_2 concentration and solvent flow rate. Higher CO_2 concentrations require deeper solvent regeneration, increasing energy demand, while higher solvent flow rates increase the mass of water that must be heated to achieve the target capture efficiency.

Similar trends are observed for the minor energy streams (Q_2, Q_4, Q_7, Q_{CO_2}, and $Q_{condenser}$), although greater relative variability is present due to their smaller magnitudes and increased sensitivity to measurement uncertainty. The desorption energy, Q_{de}, remains broadly consistent across CO_2 concentrations, reflecting similar amounts of CO_2 captured under each condition to achieve the same target capture efficiency.

The SSG ranges from 0.86 to 1.50, with an average of 1.06. For most conditions, the mass of generated steam is comparable to the mass of captured CO_2. However, SSG increases with solvent flow rate for each CO_2 concentration, confirming that an increase in water circulation leads to higher steam generation.

The uncertainty analysis complementing the system energy balance is presented in the Supplementary Materials.

6. Solvent regeneration energy

6.1. Introduction to the regeneration energy

The regeneration energy of a solvent is defined as the total energy required to convert rich solvent to lean solvent through CO_2 desorption. It is conventionally expressed as the sum of three primary contributions: sensible heat to raise the solvent temperature, the vaporisation energy associated with steam generation, and the heat of reaction for CO_2 desorption (Oexmann and Kather, 2010; Artanto et al., 2012; Nwaoha et al., 2017; Tatarczuk et al., 2024; Vinjarapu et al., 2024):

$$Q_{regen} = Q_{sens} + Q_{vap} + Q_{react} \quad (16)$$

Where:

Q_{regen} = conventional regeneration energy (kJ/h)
Q_{sens} = total sensible heat of the solvent (kJ/h)
Q_{vap} = total energy required to vaporise the solvent in the reboiler (kJ/h)
Q_{react} = total energy required for CO_2 desorption (kJ/h)

The regeneration energy demand is reduced when the internal heat recovery within the stripper is accounted for:

$$Q_{regen,net} = Q_{sens} + Q_{vap} + Q_{react} - Q_{recovery} \quad (17)$$

Where:

$Q_{regen,net}$ = net regeneration energy (kJ/h)
$Q_{recovery}$ = total energy of internal heat recovery (kJ/h)

Table 5
Energy balances across the stripper for different capture conditions.

Parameter	Units	Capture Condition												
		25_800	25_900	25_1000	25_1100	20_800	20_900	20_1000	20_1100	20_1200	15_600	15_700	15_800	10_400	10_500	10_700
Q1	MJ/h	196.8	229.7	254.2	280.9	197.9	218.1	249.1	287.8	312.5	148.9	179.6	207.6	103.1	125.0	182.9
Q2	MJ/h	0.5	0.6	0.5	0.5	0.1	0.2	0.1	0.2	0.2	0.1	0.2	0.2	0.1	0.1	0.1
Q3	MJ/h	156.5	164.7	174.8	184.5	142.7	163.3	166.8	163.2	173.3	109.0	118.7	125.9	71.7	85.1	109.7
Q4	MJ/h	7.5	8.9	8.4	8.4	6.9	6.4	7.0	8.0	8.0	5.1	5.7	6.1	3.4	3.4	3.6
Q5	MJ/h	346.3	386.0	421.1	457.5	333.8	375.2	409.0	443.2	443.2	253.0	292.8	327.6	171.4	206.6	289.0
Q6	MJ/h	316.5	354.6	384.2	415.5	305.0	338.4	369.9	402.0	433.3	229.8	264.7	298.0	158.0	189.5	260.7
Q7	MJ/h	0.5	0.6	0.5	0.5	0.1	0.2	0.1	0.1	0.2	0.2	0.1	0.1	0.1	0.1	0.1
$Q_{reboiler}$	MJ/h	255.5	260.7	257.8	260.3	210.7	223.2	229.1	227.3	234.5	154.7	162.5	171.1	111.5	108.9	127.7
$Q_{condenser}$	MJ/h	6.4	7.8	7.4	7.4	6.7	6.1	6.8	7.7	7.6	4.8	5.4	5.8	3.3	3.4	3.5
Q_{de}	MJ/h	128.9	127.4	119.9	117.8	96.8	96.6	101.4	105.3	105.9	68.8	71.9	74.8	53.3	41.0	46.3
$\dot{m}_{CO2,captured}$	kg/h	63.0	68.2	63.8	62.9	54.6	54.2	54.3	53.6	53.6	40.8	40.2	40.6	26.0	26.4	26.5
Q_{CO2}	MJ/h	6.5	7.0	6.5	6.4	5.6	5.5	5.5	5.4	5.4	4.2	4.1	4.1	2.7	2.7	2.6
$\dot{m}_{steam}$	kg/h	55.7	58.5	62.5	66.2	50.9	58.6	60.0	58.7	62.5	38.9	42.5	45.2	25.7	30.6	39.8
Q_{steam}	MJ/h	149.9	157.6	168.3	178.1	137.1	157.8	161.3	157.8	167.9	104.8	114.6	121.8	69.1	82.4	107.0
SSG	kg/kg	0.9	0.9	1.0	1.1	0.9	1.1	1.1	1.1	1.2	1.0	1.1	1.1	1.0	1.2	1.5

Under steady state conditions, the reboiler duty must satisfy the net regeneration energy and any system heat losses (Notz et al., 2012; Tatarczuk et al., 2024):

$$\boldsymbol{Q}_{\mathbf{reboiler}} = \boldsymbol{Q}_{\mathbf{regen,net}} + \boldsymbol{Q}_{\mathbf{losses}} \tag{18}$$

Where:

$\boldsymbol{Q}_{\mathbf{losses}}$ = generalised heat losses across the system (kJ/h)

Combining these terms yields the overall energy balance for solvent regeneration:

$$\boldsymbol{Q}_{\mathbf{reboiler}} = \boldsymbol{Q}_{\mathbf{sens}} + \boldsymbol{Q}_{\mathbf{vap}} + \boldsymbol{Q}_{\mathbf{react}} - \boldsymbol{Q}_{\mathbf{recovery}} + \boldsymbol{Q}_{\mathbf{losses}} \tag{19}$$

The individual contributions were evaluated using a combination of thermodynamic data from the open literature and Aspen Plus. The calculated regeneration energies for the capture conditions are presented in Table 6, with each energy component from Eq. (17) plotted as a function of the L/G ratio for each capture condition in Fig. 8. The corresponding uncertainties for each component are presented in the Supplementary Materials.

Several studies have attempted a system-level energy balance to determine the regeneration energy and its constituent components (Notz et al., 2012; Li et al., 2016; Tatarczuk et al., 2024). However, quantitative results are highly dependent on process configuration, operating conditions, and calculation methodology. As a result, direct comparison with literature values is often not meaningful. While there is broad agreement in the use of energy balance approaches, where similar methodologies are employed to determine the sensible heat, variations in the definition of vaporisation energy and the treatment of reaction enthalpy have significant implications on the resulting energy distributions. In the following sections, methodologies for calculating each energy component are outlined, with their corresponding results analysed.

6.2. Sensible heat

The sensible heat of the solvent represents the energy required to raise the rich solvent to the reboiler temperature. This is a major contribution to the overall regeneration energy and is partially offset through heat recovery in the cross-heat exchanger, which preheats the rich solvent prior to entering the stripper.

In this work, the sensible heat is divided into four contributions (Leites et al., 2003; Tatarczuk et al., 2024):

$$\boldsymbol{Q}_{\mathbf{sens}} = \boldsymbol{Q}_{\mathbf{sens,rich}} + \boldsymbol{Q}_{\mathbf{sens,column}} + \boldsymbol{Q}_{\mathbf{sens,condenser}} + \boldsymbol{Q}_{\mathbf{sens,bottom}} \tag{20}$$

Where:

$\boldsymbol{Q}_{\mathbf{sens,rich}}$ = sensible heat to get the hot rich solvent component to the stripper bottom temperature (kJ/h)
$\boldsymbol{Q}_{\mathbf{sens,column}}$ = sensible heat to get the column steam condensate to the stripper bottom temperature (kJ/h)
$\boldsymbol{Q}_{\mathbf{sens,condenser}}$ = sensible heat to get the condenser steam condensate to the stripper bottom temperature (kJ/h)
$\boldsymbol{Q}_{\mathbf{sens,bottom}}$ = sensible heat to get the total solvent at the stripper bottom to the reboiler core temperature (kJ/h)

Each term was evaluated using Eq. (4), with specific heat capacities determined at the average temperature of the respective temperature change. Values for the condensate terms were obtained using the CoolProp add-in, while values for the solvent terms were provided by Aspen Plus.

Fig. 8A presents the sensible heat as a function of L/G ratio for each capture condition, showing the expected increase with solvent flow rate across all CO_2 concentrations. This reflects the greater energy required to heat larger solvent volumes. Slightly elevated values are observed for

Table 6
Solvent regeneration energy components and other key values for different capture conditions.

Parameter	Units	Capture Condition												
		25_800	25_900	25_1000	25_1100	20_800	20_900	20_1000	20_1100	20_1200	15_600	15_700	15_800	10_400	10_500	10_700
Q_{ens}	MJ/h	113.3	119.1	126.9	133.7	103.1	118.0	121.3	118.5	125.9	78.8	85.9	91.2	52.0	61.9	80.7
$Q_{ens,rich}$	MJ/h	99.0	102.8	108.9	114.3	88.6	101.4	103.8	98.7	104.3	67.8	70.5	74.7	44.2	52.2	66.5
$Q_{ens,column}$	MJ/h	4.4	5.6	5.2	5.2	4.5	4.0	4.5	5.4	5.3	3.3	3.8	4.1	2.2	2.2	2.3
$Q_{ens,condenser}$	MJ/h	0.8	0.7	0.6	0.4	0.4	0.3	0.2	0.1	0.0	0.3	0.3	0.1	0.2	0.1	-0.1
$Q_{ens,bottom}$	MJ/h	8.9	9.8	12.0	13.6	9.5	12.2	12.6	14.1	16.2	7.2	11.2	12.1	5.2	7.1	11.9
Q_{vap}	MJ/h	123.8	130.2	139.2	147.5	113.5	130.7	133.8	131.0	139.6	86.7	94.7	100.9	57.1	68.2	89.0
Q_{react}	MJ/h	119.8	127.7	120.2	119.9	105.1	103.5	101.9	103.1	102.5	77.0	76.0	76.2	49.3	49.6	48.7
H_{abs}	kJ/mol•CO_2	83.68	82.49	82.93	83.85	84.67	84.04	82.61	84.68	84.13	83.15	83.27	82.46	83.52	82.88	80.96
$Q_{recovery}$	MJ/h	129.3	136.0	144.6	152.6	118.0	135.2	138.1	135.0	143.4	90.1	98.3	104.2	59.3	70.5	91.0
Q_{cond}	MJ/h	124.9	131.3	140.2	148.5	114.3	131.6	134.5	131.7	140.2	87.4	95.4	101.5	57.6	68.7	89.3
$Q_{CO2,cool}$	MJ/h	2.2	2.2	2.0	1.9	1.8	1.8	1.7	1.5	1.4	1.3	1.2	1.2	0.8	0.8	0.8
$Q_{ens,steam}$	MJ/h	2.3	2.5	2.4	2.3	1.9	1.9	1.9	1.9	1.8	1.5	1.6	1.6	1.0	1.0	1.0
$Q_{reboiler}$	MJ/h	255.5	260.7	257.8	260.3	210.7	223.2	229.1	227.3	234.5	154.7	162.5	171.1	111.5	108.9	127.7
$Q_{regen,net}$	MJ/h	227.6	241.0	241.6	248.4	203.7	217.0	218.9	217.6	224.5	152.4	158.3	163.9	99.1	109.2	127.2
Q_{losses}	MJ/h	27.9	19.7	16.1	11.8	7.0	6.2	10.2	9.7	10.0	2.3	4.2	7.2	12.4	-0.3	0.5
Q_{losses}	% of $Q_{reboiler}$	10.92	7.56	6.26	4.55	3.33	2.77	4.45	4.26	4.28	1.49	2.59	4.21	11.11	-0.31	0.39

cases 20_900 and 20_1000, attributed to marginally lower stripper top temperatures, increasing the heating required to reach the reboiler temperature.

Higher flue gas CO_2 concentrations also increase sensible heat demand. Increasing CO_2 concentration requires lower lean loadings to align the solvent cyclic capacity with the target capture efficiency, as shown in Table 4, which increases the relative fraction of MEA and water in the solvent. This effectively increases the mass of solvent requiring heating. Additionally, higher CO_2 concentrations result in greater captured CO_2 mass in the rich solvent, as shown in Table 5, further contributing to the sensible heat requirement.

Previous studies have shown that enhanced heat integration through advanced process modifications, such as absorber intercooling (Tobiesen et al., 2007; Karimi et al., 2011; Le Moullec et al., 2014), rich solvent splits (Le Moullec and Kanniche, 2011; Xue et al., 2017), solvent split flows (Shoeld, 1934; Chang and Shih, 2005; Ahn et al., 2013; Le Moullec et al., 2014), lean vapour compression (Reddy et al., 2009; Woodhouse and Rushfeldt, 2010; Le Moullec and Kanniche, 2011; Xue et al., 2017), can reduce sensible heat demand and enhance overall energy efficiency (Sultan et al., 2021).

6.3. Vaporisation energy

The vaporisation energy is the energy required to generate steam in the reboiler. This steam serves a critical physical function: as it rises through the stripper column, it reduces the partial pressure of CO_2 in the vapour phase. According to vapour-liquid equilibrium principles, this increases the driving force for CO_2 desorption, facilitating easier solvent regeneration (Notz et al., 2012; Mullen et al., 2024). Upon condensation, the steam releases latent heat, which contributes to heating the rich solvent and driving the desorption reaction.

The vaporisation energy is calculated as:

$$\boldsymbol{Q}_{\mathbf{vap}} = \dot{\boldsymbol{m}}_{\mathbf{steam}} \cdot \boldsymbol{h}_{\mathbf{fg}} \tag{21}$$

Where:

$\boldsymbol{h}_{\mathbf{fg}}$ = specific enthalpy of vaporisation/condensation (kJ/kg)

Fig. 8B presents the vaporisation energy as a function of L/G ratio for each capture condition, exhibiting trends and magnitudes comparable to those observed for sensible heat in Fig. 8A. Vaporisation energy increases with solvent flow rate, as higher flows lead to a larger volume of water and increased steam production, as shown in Table 5. It also increases with flue gas CO_2 concentration, reflecting the greater steam requirement to achieve deeper solvent regeneration at higher CO_2 concentrations. Cases 20_900 and 20_1000 again show slightly elevated values, attributed to increased steam generation. Minimising vaporisation energy is primarily achieved through process optimisation. Operating as close as possible to the stripper inflection point limits excessive steam production and reduces vapour losses overhead (Gibbins, 2023). While steam generation is inherently required for solvent regeneration, optimal operation promotes effective condensation within the column, thereby reducing the overall vaporisation energy demand.

6.4. Desorption energy

The liberation of CO_2 from MEA is an endothermic process, and it is commonly assumed that the heat of desorption, also known as reaction enthalpy, is equal in magnitude to the heat of absorption (Oexmann and Kather, 2010; Nwaoha et al., 2017; Tatarczuk et al., 2024). The reaction enthalpy has been widely studied (Jou et al., 1994; Kim and Svendsen, 2007; McCann et al., 2008; Kim et al., 2009, 2014; Chowdhury et al., 2011; Liu et al., 2012; Arshad et al., 2013; Wanderley et al., 2020; Vinjarapu et al., 2024), showing strong dependence on variables such as

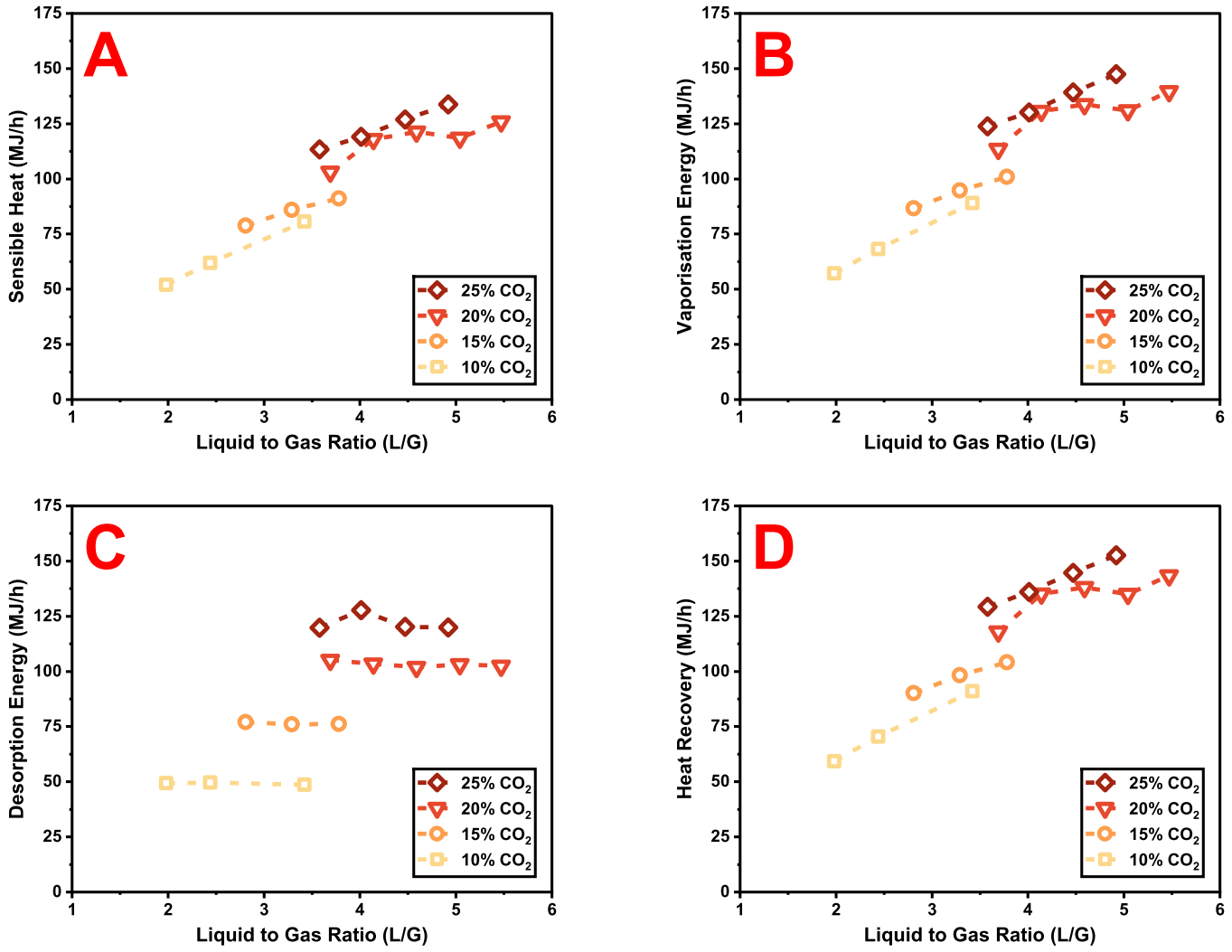

Fig. 8. (A) sensible heat, (B) vaporisation energy, (C) desorption energy, and (D) heat recovery against liquid to gas ratio for solvent flow rates treating 150 Nm^3/h flue gas containing different CO_2 concentrations, targeting 90% capture efficiency.

solvent type, concentration, loading, temperature, pressure, and the presence of additives. While its quantification is important for understanding solvent performance, reducing this energy requirement is challenging. Alternative solvents, including piperazine (Liu et al., 2012), hindered amines (Chowdhury et al., 2011), tertiary amines (Arshad et al., 2013), and solvent blends (Mangalapally et al., 2012; Mun et al., 2022), have demonstrated lower reaction enthalpies than MEA, though often with trade-offs in performance or operability. Proprietary solvents such as KS-1™ by Mitsubishi Heavy Industries (Miyamoto et al., 2017) and APBS-CDRMax® by Carbon Clean Solutions Limited (Frimpong et al., 2021), have also shown improved performance relative to MEA.

In this study, the heat of desorption is based on the experimental data of Kim et al. (2014), widely regarded as a benchmark for MEA systems, with specific reference to their data for a 30 wt.% MEA solution. Their results show that the reaction enthalpy increases with temperature for a fixed solvent loading, enabling interpolation at intermediate temperatures. For loadings above 0.25, the reaction enthalpy becomes largely independent of MEA concentration, supporting comparison with the 35 wt.% MEA used in this study. For loadings above 0.5, the enthalpy decreases significantly due to the transition from chemical absorption to physical dissolution.

For the conditions investigated in this study, lean loadings are generally above 0.25 and rich loadings lie between 0.5 and 0.55. As a result, the average heat of desorption depends on the initial rich loading and extent of regeneration, as regeneration begins in a lower-enthalpy regime and progresses towards higher values as loading decreases. The average heat of desorption for each condition was estimated using the 80°C dataset from Kim et al. (2014), based on the measured lean and rich loadings and the total CO_2 absorbed. A segmental integration approach was applied across discretised loading intervals, using tabulated or interpolated values to calculate the total reaction energy. The resulting average heats of desorption ranged from 80.96 to 84.68 kJ/mol•CO_2, consistent with the trends reported by Kim et al. (2014), supporting the validity of this approach.

The desorption energy is then calculated as:

$$\boldsymbol{Q}_{\text{react}} = \frac{\dot{\boldsymbol{m}}_{\text{CO}_2,\ \text{captured}}}{\boldsymbol{MW}_{\text{CO}_2}} \cdot \boldsymbol{H}_{\text{abs}} \tag{22}$$

Where:

$\boldsymbol{H}_{\text{abs}}$ = average specific enthalpy of desorption (kJ/mol•CO_2)

Fig. 8C presents the desorption energy as a function of L/G ratio for each capture condition and is used to assess the validity of the applied methodology. For a given CO_2 concentration, the reaction energy is expected to remain broadly consistent across solvent flow rates, as a similar quantity of CO_2 is liberated from the solvent. This behaviour is

observed for the 10, 15, and 20 mol.% CO_2 conditions. For the 25 mol.% condition, only the 25_900 case achieved the target 90% capture efficiency, while the remaining conditions achieved approximately 84 to 87%, resulting in correspondingly lower desorption energies.

Desorption energy increases with CO_2 concentration, reflecting the greater quantity of CO_2 released from the solvent. The step change in average desorption energy between successive concentrations is consistent, indicating a near-linear relationship between CO_2 concentration and desorption energy for a set capture efficiency. The difference between the 20 mol.% conditions and the 25_900 case further reinforces this conclusion.

A comparison between the directly calculated desorption energy, $\boldsymbol{Q}_{\mathbf{react}}$, and the indirect values obtained from the energy balance, $\boldsymbol{Q}_{de}$, shows good agreement across the capture conditions, as illustrated in Fig. 9.

6.5. Heat recovery

The total heat recovery within the stripper is divided into three contributions, dominated by latent heat release from steam condensation within the column. As steam rises, it progressively condenses, transferring latent heat to the downflowing rich solvent. Additional, smaller contributions arise from sensible heat transfer as both steam and liberated CO_2 cool while ascending the column. The heat recovery in this work is therefore expressed as:

$$\boldsymbol{Q}_{\mathbf{recovery}} = \boldsymbol{Q}_{\mathbf{cond}} + \boldsymbol{Q}_{\mathbf{sens,CO_2}} + \boldsymbol{Q}_{\mathbf{sens,steam}} \tag{23}$$

Where:

$\boldsymbol{Q}_{\mathbf{cond}}$ = latent heat released from condensing steam within the column (kJ)
$\boldsymbol{Q}_{\mathbf{sens,CO_2}}$ = sensible heat transferred from the cooling of CO_2 within the column (kJ)
$\boldsymbol{Q}_{\mathbf{sens,steam}}$ = sensible heat transferred from the cooling of steam within the column (kJ)

$$\boldsymbol{Q}_{\mathbf{cond}} = \dot{\boldsymbol{m}}_{\mathbf{steam,cond}} \cdot \boldsymbol{h}_{\mathbf{fg}} \tag{24}$$

The latent heat contribution, $\boldsymbol{Q}_{\mathbf{cond}}$, is calculated from the mass of steam condensed within the column and the enthalpy of condensation at the saturation temperature:

The sensible heat contribution from CO_2 cooling, $\boldsymbol{Q}_{\mathbf{sens,CO_2}}$, is evaluated between the reboiler temperature and the column top temperature with Eq. (4), using an average specific heat capacity. The sensible heat contribution from steam is resolved into two components:

$$\boldsymbol{Q}_{\mathbf{sens,steam}} = \boldsymbol{Q}_{\mathbf{column,steam}} + \boldsymbol{Q}_{\mathbf{top,H_2O}} \tag{25}$$

Where:

$\boldsymbol{Q}_{\mathbf{column,steam}}$ = sensible heat transferred from the steam cooling to the saturation temperature (kJ/h)
$\boldsymbol{Q}_{\mathbf{top,H_2O}}$ = sensible heat transferred from the water that exits the top of the stripper (kJ/h)

Both terms are evaluated using Eq. (4) using temperature differences across the respective regions with specific heat capacities taken at average temperatures.

Fig. 8D presents the total heat recovery energy as a function of L/G ratio for each capture condition, with trends closely aligning with those of the vaporisation energy shown in Fig. 8B. This is expected, as the generated heat is assumed to transfer its latent heat to the descending rich solvent as it condenses within the column. As a result, $\boldsymbol{Q}_{\mathbf{vap}}$ and $\boldsymbol{Q}_{\mathbf{recovery}}$ functionally offset one another, reflecting internal energy redistribution through phase change.

Heat recovery from the sensible cooling of CO_2 and steam is small in comparison to that from steam condensation, with the combined sensible contributions accounting for less than 4% of the latent heat term. While minor, these contributions remain important for closure of the overall energy balance and accurate estimation of system heat losses. The total heat recovery is always slightly in excess of the vaporisation energy for each condition.

6.6. System heat loss

With all components of the net regeneration energy, $\boldsymbol{Q}_{\mathbf{regen,net}}$, evaluated, their sum can be compared with the calculated reboiler duty, $\boldsymbol{Q}_{\mathbf{reboiler}}$. For a consistent energy balance, the net regeneration energy is expected to be less than the reboiler duty for each capture condition, with the difference corresponding to the generalised heat loss of the system. The results of this comparison are presented in Fig. 10.

As shown in Fig. 10, the calculated net regeneration energy closely follows the reboiler duty and is slightly lower in most cases, consistent with the presence of heat losses within the system. The agreement between these values supports the validity of the methodology, with further confidence provided by the associated uncertainty analysis. The generalised heat loss can be estimated by rearranging Eq. (18):

$$\boldsymbol{Q}_{\mathbf{losses}} = \boldsymbol{Q}_{\mathbf{reboiler}} - \boldsymbol{Q}_{\mathbf{regen,net}} \tag{26}$$

The calculated heat losses range from -0.3 to 27.9 MJ/h, with an average of 9.7 MJ/h. Expressed as a percentage of the reboiler duty, the values range from -0.31 to 11.11%, with an average of 4.52%. Negative values are not physically meaningful and arise from measurement

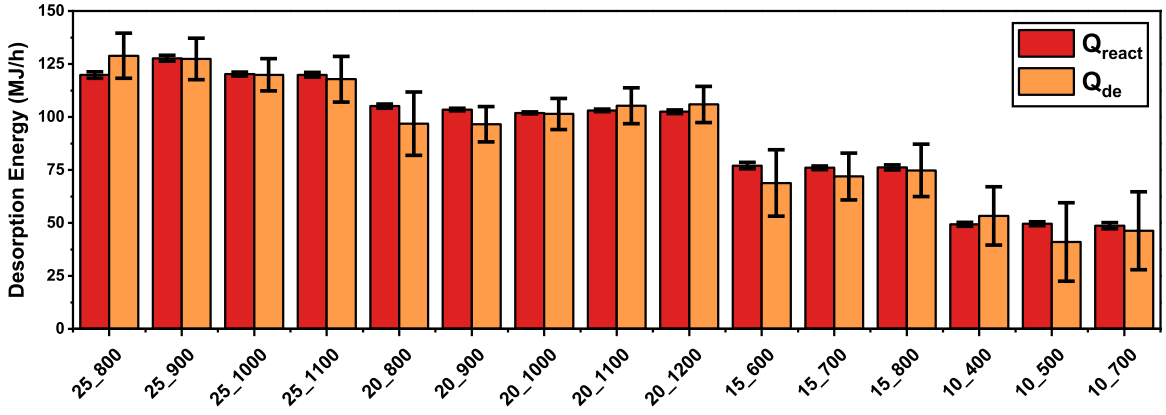

Fig. 9. Comparison of desorption energy values given by Q_{react} and Q_{de} for different capture conditions. Error bars represent the propagated combined standard uncertainty (±1σ) for each value.

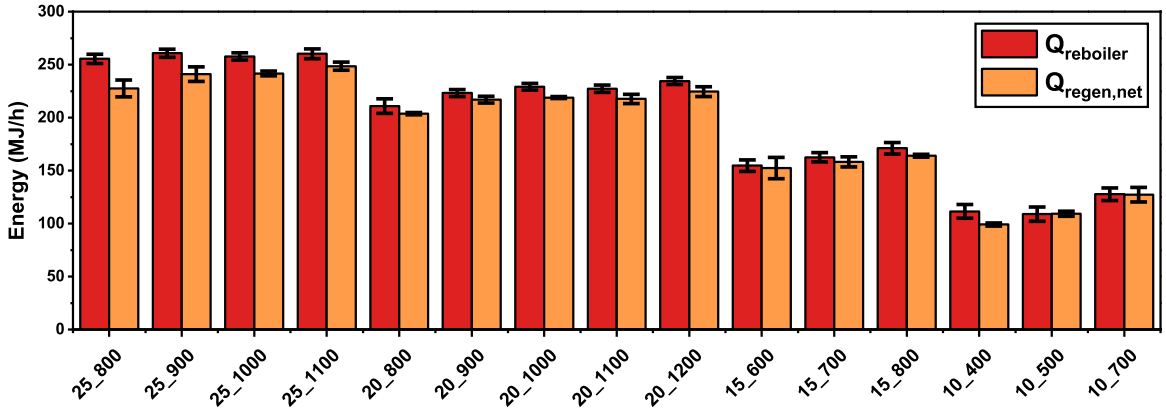

Fig. 10. Comparison of energy values given by $Q_{reboiler}$ and $Q_{regen,net}$ for different capture conditions. Error bars represent the propagated combined standard uncertainty (±1σ) for each value.

uncertainty, reflecting the sensitivity of the calculation to propagated uncertainties, discussed further in the Supplementary Materials. The relatively small magnitude of the calculated heat losses supports the validity of the overall energy balance, indicating that the dominant energy contributions have been appropriately accounted for.

These values are lower than those typically reported in the literature, where heat losses of 15–35% of reboiler duty are common for pilot-scale systems (Notz et al., 2012; Suresh Babu and Rochelle, 2021; Tatarczuk et al., 2024). This discrepancy is attributed primarily to plant scale and methodology. Larger systems generally exhibit lower relative heat losses due to reduced surface area-to-volume ratios, while indirect estimation methods, as applied here, capture net system losses rather than losses associated with specific equipment. Overall, the results indicate that heat losses in the EIC ACP are modest relative to the total energy demand, although their precise quantification would require a dedicated investigation.

6.7. Regeneration energy distribution

With the individual energy contributions established, the conventional regeneration energy, $\boldsymbol{Q_{regen}}$, was analysed to assess the relative contributions of sensible heat, vaporisation energy, and desorption energy. The corresponding energy distributions are presented in Fig. 11.

Fig. 11 shows that the relative components are broadly consistent across capture conditions. Vaporisation energy is the dominant component in all cases, followed by sensible heat, while the heat of desorption represents the smallest contribution.

As the solvent flow rate increases for a given CO_2 concentration, the distribution between the terms becomes more pronounced. The values of $\boldsymbol{Q_{sens}}$ and $\boldsymbol{Q_{vap}}$ increase substantially due to the increased mass of solvent requiring heating and steam generation. In contrast, $\boldsymbol{Q_{react}}$, remains comparatively stable, reflecting the consistent CO_2 capture.

These results highlight the importance of system optimisation for a chosen solvent, where improvements in regeneration energy are primarily made by reducing the sensible heat and vaporisation energy. Sensible heat can be minimised through enhanced heat integration, where advanced process configurations can improve the preheating of the rich solvent entering the stripper. Vaporisation energy is best reduced by operating at the stripper inflection point, limiting excess steam generation. Consequently, effective optimisation requires a combined approach targeting both heat integration and operating conditions.

7. Conclusions

This study has presented a comprehensive pilot-scale experimental investigation of MEA-based post-combustion carbon capture under elevated flue gas CO_2 concentrations representative of industrial process emissions such as steelmaking. The work provides a novel experimentally validated dataset for CO_2 concentrations up to 25 mol.% using a conventional PB absorber with 35 wt.% MEA, addressing a recognised gap in pilot-scale performance data under these conditions. As such, it establishes a practical baseline for benchmarking and future development of industrial chemical absorption systems.

The experimental results demonstrated that the expected relationships between L/G ratio, solvent loading, column temperature profiles, and SRD remained valid at elevated CO_2 concentrations. An optimal operating condition was identified for 25 mol.% CO_2 flue gas at an L/G ratio of 4.01 and an SRD of 3.83 MJ/kg•CO_2. This condition reflects a balance between the energy required for solvent circulation and solvent

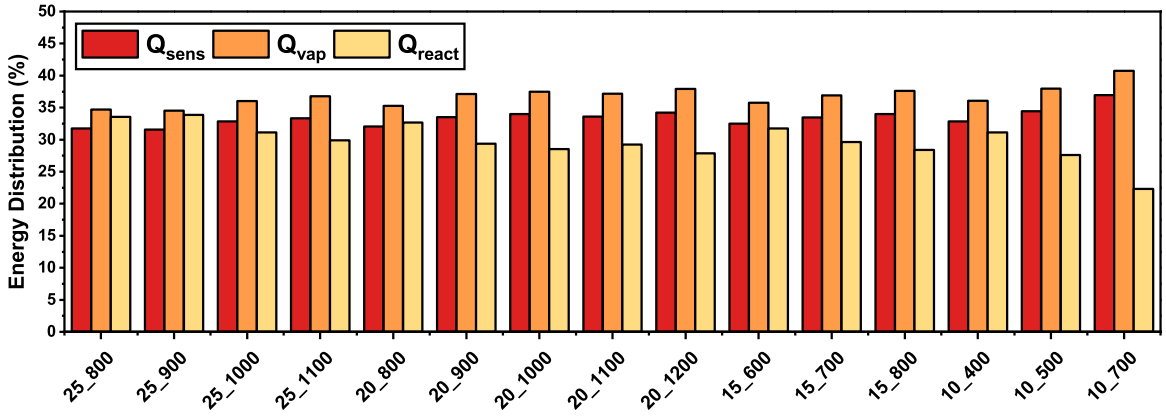

Fig. 11. Energy distribution of Q_{sens}, Q_{vap}, and Q_{react} as percentages of the conventional regeneration energy for different capture conditions.

regeneration, minimising the overall regeneration energy demand. The measured temperature profiles further demonstrated their value as practical operational diagnostics, providing insight into absorber and stripper operating regimes and the location of dominant mass transfer activity during continuous operation.

A detailed component-level breakdown of regeneration energy was developed through application of the overall system energy balance. The study provides a transparent methodology for identifying the principal contributors to regeneration energy demand by incorporating sensible heat, vaporisation energy, desorption energy, heat recovery, and heat losses within a consistent analytical framework. This will assist future optimisation efforts of conventional PB absorption systems and provide the foundations for improving capture performance.

The indirect estimation of system heat losses indicates that the overall energy balance is well resolved, with relatively low losses compared to typical pilot-scale systems. However, the results also highlight the limitations of indirect methods and the influence of uncertainty propagation, reinforcing the need for careful interpretation of process data and derived energy metrics.

The present work was intentionally focused on establishing experimental performance benchmarks under controlled operating conditions using fresh solvent and synthetic flue gas. Consequently, long-term effects associated with solvent degradation, corrosion, and solvent management, were not considered. Likewise, the study was not intended to provide detailed rate-based modelling of gas-liquid mass transfer or a techno-economic assessment of industrial implementation. Future work should therefore build upon the experimental dataset presented here through detailed process modelling, long-term degradation studies under representative industrial flue gas compositions, and integrated techno-economic assessment incorporating solvent management, equipment design, utility requirements, and process integration.

Overall, this work provides both a novel experimental dataset and a transferable analytical framework for evaluating chemical absorption performance at elevated CO_2 concentrations relevant to hard-to-abate industries. These results provide a robust foundation for future development of advanced solvents, process intensification strategies, and scale-up of chemical absorption systems for industrial decarbonisation.

Declaration of generative AI and AI-assisted technologies in the manuscript preparation process

During the preparation of this work the authors used ChatGPT and Gemini in order to improve readability and refine the language of the manuscript. After using these tools, the authors reviewed and edited the content as needed and take full responsibility for the content of the published article.

CRediT authorship contribution statement

Jack Wells: Writing – original draft, Visualization, Validation, Methodology, Investigation, Formal analysis, Conceptualization. **Muhammad Akram:** Writing – review & editing, Supervision, Resources, Methodology, Investigation. **Andy Heeley:** Writing – review & editing, Validation, Supervision. **Kevin J. Hughes:** Writing – review & editing, Supervision. **Derek B. Ingham:** Writing – review & editing, Project administration. **Mohamed Pourkashanian:** Supervision, Resources, Project administration, Funding acquisition.

Declaration of competing interest

The authors declare that they have no known competing financial interests or personal relationships that could have appeared to influence the work reported in this paper.

Acknowledgements

This research was supported by the Centre for Doctoral Training (CDT) in Resilient Decarbonised Fuel Energy Systems (RDFES), funded by the Engineering and Physical Sciences Research Council (EPSRC) under Grant No. EP/S022996/1, with additional financial support provided by the Centre for Research into Energy Demand Solutions (CREDS) and the International Flame Research Foundation (IFRF). The experimental work was conducted using the facilities of the Energy Innovation Centre (EIC) at the University of Sheffield, funded by the European Regional Development Fund (ERDF), Brussels, Belgium, and the Department for Energy Security and Net Zero (DESNZ).

Supplementary materials

Supplementary material associated with this article can be found, in the online version, at doi:10.1016/j.ccst.2026.100659.

Appendices

A. *Supplementary experimental result analyses*

A.1. *20% CO_2 flue gas capture conditions*

Key performance metrics for conditions with a flue gas CO_2 concentration of 20 mol.% are shown in Fig. A.1.

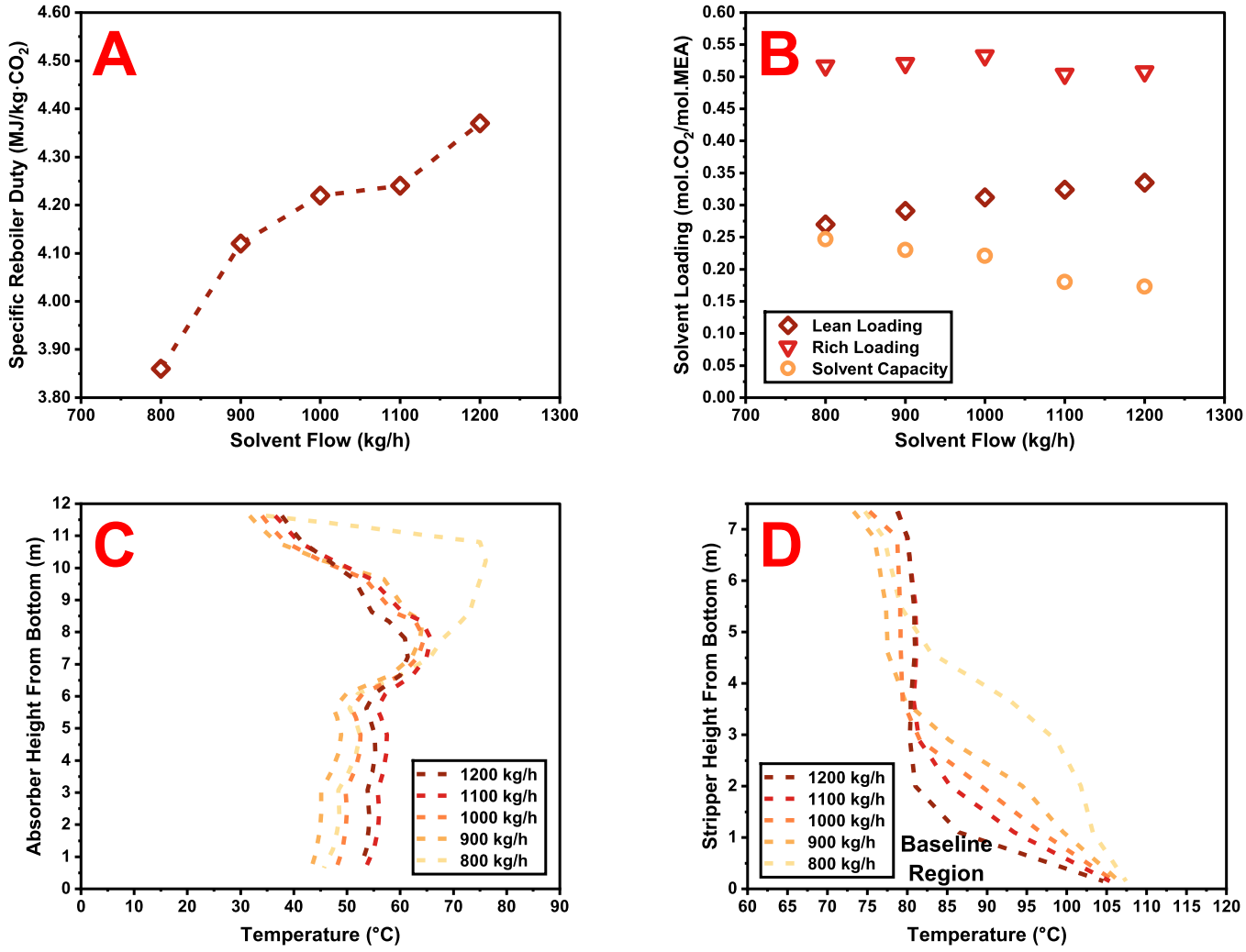

Fig. A.1. Key performance metrics for solvent flow rates treating 150 Nm^3/h flue gas containing 20 mol.% CO_2, targeting 90% capture efficiency: (A) specific reboiler duty, (B) solvent loadings and capacity, (C) absorber temperature profiles, and (D) stripper temperature.

The tested solvent flow rate range for 20 mol.% CO_2 matched that used for 25 mol.% CO_2. As shown in Fig. A.1A, the optimal L/G ratio was not clearly identified, as SRD continued to decrease with decreasing solvent flow. At the lowest tested flow rate of 800 kg/h, an SRD of 3.86 MJ/kg•CO_2 was recorded, comparable to the minimum value of 3.83 MJ/kg•CO_2 at 900 kg/h for the 25 mol.% condition. This supports DCC model predictions that optimal SRD values are similar across varying CO_2 concentrations (Wells et al., 2025). While this suggests that 800 kg/h is near the optimal condition, the true minimum likely lies below the tested range. All tested flow rates achieved approximately 90% capture efficiency, where the reboiler operated below the maximum heat input.

The solvent loadings shown in Fig. A.1B typically follow expected trends, with lean loading increasing and rich loading decreasing slightly with solvent flow rate. Lean loadings range from 0.270 to 0.335, while rich loadings range from 0.533 to 0.504, consistent with reduced residence time and physical dissolution at higher flow rates. The rich loading value at 1000 kg/h appears anomalously high. Overall, solvent cyclic capacity decreases with increasing solvent flow rate. Notably at 800 kg/h the lean loading is 0.270, approaching the DCC prediction of 0.260 for optimal operation (Wells et al., 2025), supporting the inference that this condition is near optimal. Extrapolation of the observed trend suggest the true optimum occurs at a slightly lower flow rate, around 750 kg/h.

The absorber temperature profiles in Fig. A.1C show convergence towards a bulge-pinched profile for flow rates between 900 and 1200 kg/h, contrasting with the 800 kg/h condition which exhibits a rich-pinched profile. Comparison with a secondary 800 kg/h condition (not reported), showed a profile consistent with higher flow rates, and implied a sensitivity to capture efficiency. The reported condition achieved 91.39% capture, compared to approximately 89% for the secondary case. Higher capture efficiencies reduce the partial pressure of CO_2 in the flue gas, making it increasingly difficult to capture. This shifts the reaction zone upwards and increases the local heat release, producing the observed rich-pinched profile. As with the 25 mol.% CO_2 conditions, the minimal temperature variation is observed in absorber 1, indicating that most absorption occurs in absorber 2.

The stripper temperature profiles in Fig. A.1D show consistent baseline operation, with operation approaching the inflection point as solvent flow decreases. Higher flow rates ≥900 kg/h move the system further into the baseline region, increasing SRD due to the energy required to heat larger solvent volumes. The 800 kg/h condition lies close to the inflection point but remains above the optimum, consistent with the lean loading trend.

A.2. 15% CO_2 flue gas capture conditions

Key performance metrics for conditions with a flue gas CO_2 concentration of 15 mol.% are shown in Fig. A.2.

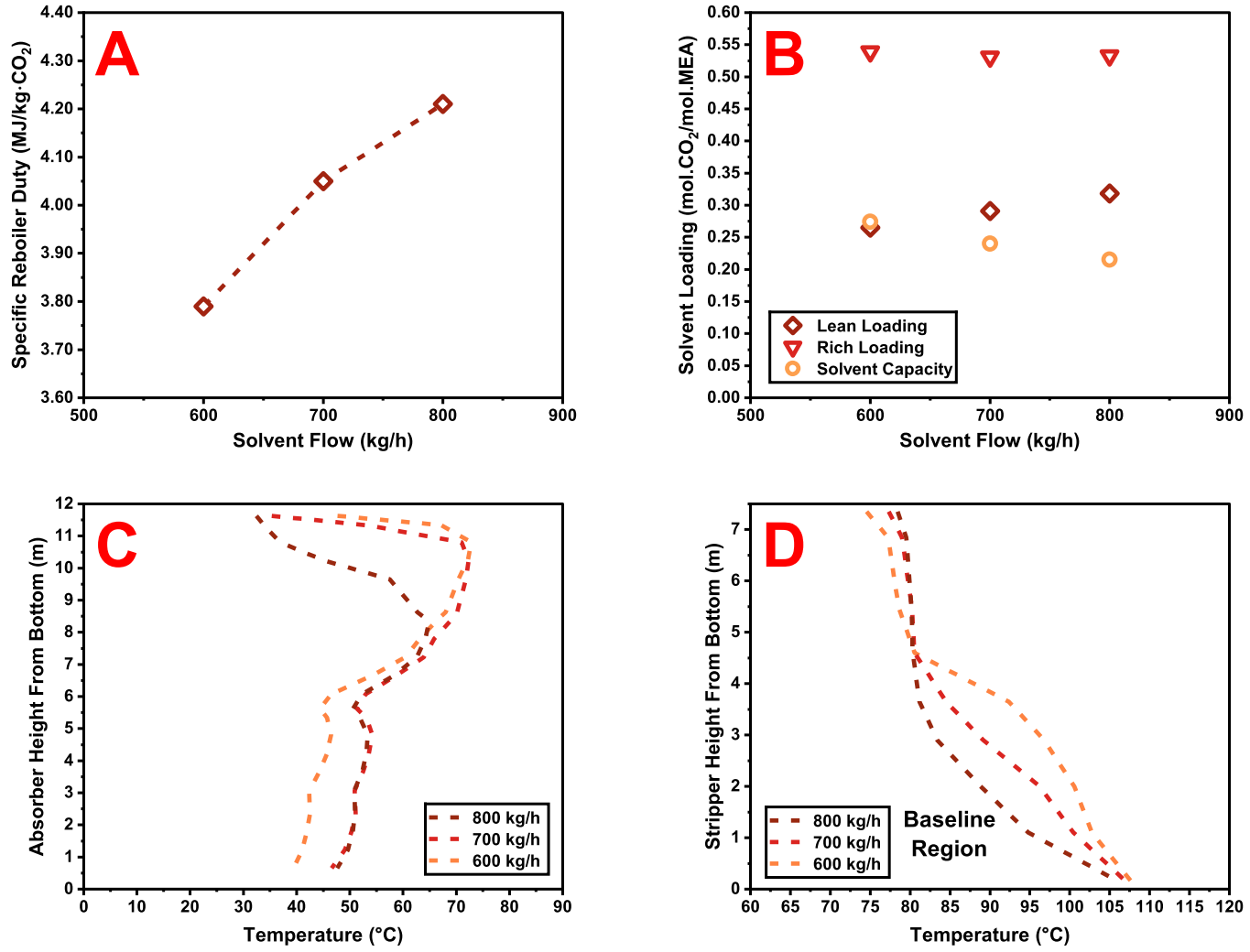

Fig. A.2. Key performance metrics for solvent flow rates treating 150 Nm^3/h flue gas containing 15 mol.% CO_2, targeting 90% capture efficiency: (A) specific reboiler duty, (B) solvent loadings and capacity, (C) absorber temperature profiles, and (D) stripper temperature.

The tested solvent flow rates for the 15 mol.% CO_2 condition were limited to three cases, as shown in Fig. A.2A. Similar to the 20 mol.% CO_2 results, the optimal L/G ratio was not clearly captured within the tested range. The lowest SRD recorded was 3.79 MJ/kg•CO_2 at a solvent flow of 600 kg/h, which may approximate the minimum, although the limited number of data points prevents a definitive conclusion. As expected, increasing the solvent flow rate above 600 kg/h resulted in higher SRD values. All three conditions achieved or exceeded the target 90% capture efficiency.

The solvent loadings in Fig. A.2B follow expected trends. Lean solvent loading increases steadily with solvent flow from 0.265 to 0.318, while rich solvent decreases slightly from 0.539 to 0.533, with some variation. Solvent cyclic capacity decreases with increasing flow, consistent with reduced regeneration extent at higher circulation rates. The DCC model predicts an optimal lean loading of approximately 0.270 for 15 mol.% CO_2 (Wells et al., 2025), while the measured value at 600 kg/h was 0.265, indicating close agreement with the model and suggesting that the minimum SRD may occur at a slightly higher solvent flow rate. However, this is not supported by the stripper temperature profiles in Fig. A.2D, which indicate that all tested conditions $\geq$600 kg/h lie within the baseline region. The inflection point has therefore not yet been reached, with extrapolation of the temperature trend suggesting that a solvent flow rate of 500 kg/h could approximate the inflection point and thus minimise SRD for the 15 mol.% CO_2 condition.

The absorber temperature profiles in Fig. A.2C reinforce earlier observations. At solvent flow rates of 600 and 700 kg/h, the system operates in a rich-pinched state, shifting towards a bulge-pinched profile at higher flow rates. As in previous cases, minimal temperature variation is observed in absorber 1, indicating that most CO_2 absorption occurs in absorber 2.

A.3. 10% CO_2 flue gas capture conditions

Key performance metrics for conditions with a flue gas CO_2 concentration of 10 mol.% are shown in Fig. A.3.

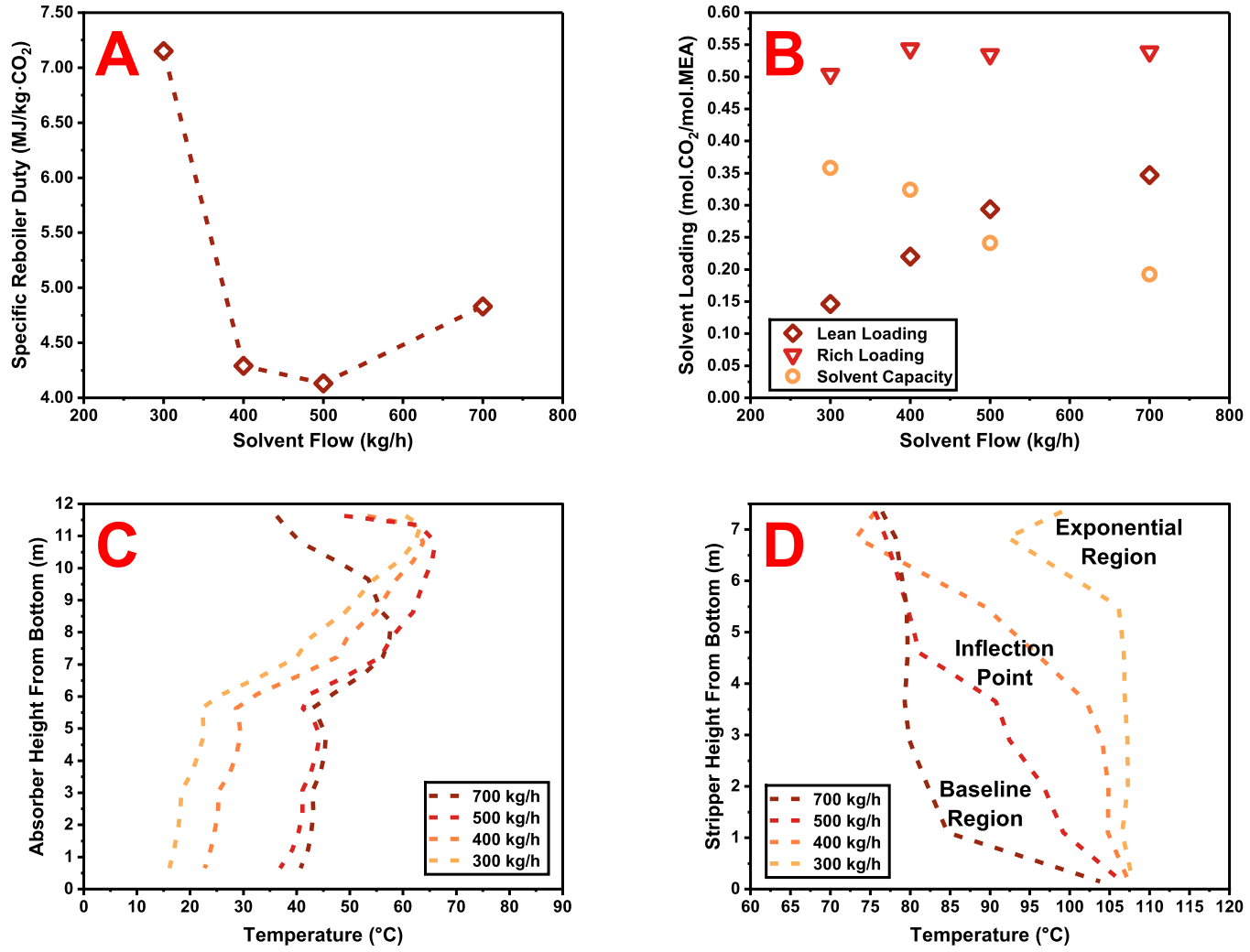

Fig. A.3. Key performance metrics for solvent flow rates treating 150 Nm^3/h flue gas containing 10 mol.% CO_2, targeting 90% capture efficiency: (A) specific reboiler duty, (B) solvent loadings and capacity, (C) absorber temperature profiles, and (D) stripper temperature.

The tested solvent flow rates for the 10 mol.% CO_2 condition spanned the lower operating range of the plant, from 700 to 300 kg/h, where all flow rates approximated 90% capture efficiency. As shown in Fig. A.3A, the minimum SRD was 4.13 MJ/kg•CO_2 at a solvent flow rate 500 kg/h, corresponding to an L/G ratio of 2.44 with a lean solvent concentration of 30.67 wt.% MEA. The minimum SRD is higher than those observed with elevated flue gas CO_2 concentrations, consistent with DCC model predictions (Wells et al., 2025), reflecting the increased energy penalty associated with capture from more dilute flue gas streams. Similar behaviour has been reported by Akram et al. (2016).

The rich solvent loadings in Fig. A.3B appear to show a deviation from trends at higher CO_2 concentrations, where loadings gradually increase with solvent flow, ranging from 0.504 to 0.544. However, this is because the value at 300 kg/h appears anomalously low, inconsistent with both the observed cyclic capacity trend and the expected increase in residence time for lower flow rates, which would favour higher CO_2 loading. Extrapolation suggests a rich loading closer to 0.550 at this condition, which would then present the expected rich loading trend. Despite this, the inverse relationship between solvent capacity and flow rate is maintained. The lean loadings range from 0.146 to 0.347. Notably, the lean loading of 0.294 at 500 kg/h matches the optimum predicted by the DCC model (Wells et al., 2025), supporting this condition as near-optimal.

The absorber temperature profiles in Fig. A.3C follow the expected operating transition. At 300 and 400 kg/h, the system exhibits rich-pinched behaviour, shifting towards a bulge-pinched profile above 500 kg/h as the reaction zone moves lower in the column. As in previous cases, absorber 1 shows minimal variation, indicating that most CO_2 absorption occurs in absorber 2.

Fig. A.3D shows all three stripper operating regions tested range. The 500 kg/h condition lies near the inflection point, with 400 kg/h entering the exponential region and 300 kg/h operating well within it, while 700 kg/h remains in the baseline region. The elevated SRD at 300 kg/h is attributed to excessive steam generation during solvent regeneration, increasing the energy demand. A distinct temperature dip at approximately 7 m is observed for the 300 and 400 kg/h conditions. This is attributed to cold condensate from the reflux condenser mixing with the hot rich solvent near the measurement point. The effect is more pronounced at lower flow rates due to relatively higher condensate fractions and is not evident at higher flows.

References

Ahn, H., Luberti, M., Liu, Z., Brandani, S., 2013. Process configuration studies of the amine capture process for coal-fired power plants. Int. J. Greenh. Gas Control 16, 29–40. https://doi.org/10.1016/j.ijggc.2013.03.002.

Akram, M., Ali, U., Best, T., Blakey, S., Finney, K.N, Pourkashanian, M., 2016. Performance evaluation of PACT Pilot-plant for CO2 capture from gas turbines with exhaust gas recycle. Int. J. Greenh. Gas Control 47, 137–150. https://doi.org/10.1016/j.ijggc.2016.01.047.

Akram, M., Gheit, A., Milkowski, K., Gale, W., Pourkashanian, M., 2025a. Comparison of conventional and process intensified next generation RPB absorbers for decarbonisation of the steel industry. Fuel 388, 134484. https://doi.org/10.1016/j.fuel.2025.134484.

Akram, M., Gheit, A., Milkowski, K., Gale, W., Pourkashanian, M., 2025b. Comparison of conventional and process intensified next generation RPB absorbers for decarbonisation of the steel industry. Fuel 388, 134484. https://doi.org/10.1016/j.fuel.2025.134484.

Akram, M., Milkowski, K., Gibbins, J., Pourkashanian, M., 2021. Controlling capture plants to avoid CO2 emissions penalties during peak load demand. Int. J. Greenh. Gas Control 106, 103285. https://doi.org/10.1016/J.IJGGC.2021.103285.

Akram, M., Milkowski, K., Gibbins, J., Pourkashanian, M., 2020. Comparative energy and environmental performance of 40 % and 30 % monoethanolamine at PACT pilot plant. Int. J. Greenh. Gas Control 95, 102946. https://doi.org/10.1016/j.ijggc.2019.102946.

Aliyu, A.A, Akram, M., Hughes, K.J, Ma, L., Ingham, D.B, Pourkashanian, M., 2021. Investigation into simulating selective exhaust gas recirculation and varying pressurized hot water temperature on the performance of the pilot-scale advanced CO2 capture plant with 40 wt(%) MEA. Int. J. Greenh. Gas Control 107, 103287. https://doi.org/10.1016/j.ijggc.2021.103287.

Arshad, M.W, von Solms, N., Thomsen, K., Svendsen, H.F, 2013. Heat of absorption of CO2 in aqueous solutions of DEEA, MAPA and their mixture. Energy Procedia 37, 1532–1542. https://doi.org/10.1016/j.egypro.2013.06.029.

Artanto, Y., Jansen, J., Pearson, P., Do, T., Cottrell, A., Meuleman, E., et al., 2012. Performance of MEA and amine-blends in the CSIRO PCC pilot plant at Loy Yang power in Australia. Fuel 101, 264–275. https://doi.org/10.1016/j.fuel.2012.02.023.

AspenTech. Aspen Plus V11 2026.

Bell, I.H, Wronski, J., Quoilin, S., Lemort, V., 2014. Pure and pseudo-pure fluid thermophysical property evaluation and the open-source thermophysical property library CoolProp. Ind. Eng. Chem. Res. 53, 2498–2508. https://doi.org/10.1021/ie4033999.

Biermann, M., Normann, F., Johnsson, F., Hoballah, R., Onarheim, K., 2022. Capture of CO2 from steam reformer flue gases using monoethanolamine: pilot plant validation and process design for partial capture. Ind. Eng. Chem. Res. 61, 14305–14323. https://doi.org/10.1021/acs.iecr.2c02205.

Brigman, N., Shah, M.I, Falk-Pedersen, O., Cents, T., Smith, V., De Cazenove, T., et al., 2014. Results of amine plant operations from 30 wt% and 40 wt% aqueous MEA testing at the CO2 technology Centre Mongstad. Energy Procedia 63, 6012–6022. https://doi.org/10.1016/j.egypro.2014.11.635.

Chang, H., Shih, C., 2005. Simulation and optimization for power plant flue gas CO 2 absorption-stripping systems. Sep. Sci. Technol. 40, 877–909. https://doi.org/10.1081/SS-200048014.

Chen, G., Chen, G., Cao, F., Zhang, R., Gao, H., Liang, Z., 2020. Mass transfer performance and correlation for CO2 absorption into aqueous 3-diethylaminopropylamine solution in a hollow fiber membrane contactor. Chem. Eng. Process. Process Intensif. 152, 107932. https://doi.org/10.1016/j.cep.2020.107932.

Chowdhury, F.A, Okabe, H., Yamada, H., Onoda, M., Fujioka, Y., 2011. Synthesis and selection of hindered new amine absorbents for CO2 capture. Energy Procedia 4, 201–208. https://doi.org/10.1016/j.egypro.2011.01.042.

Climate Change Committee. The seventh carbon budget. 2025.

Davis, J., Rochelle, G., 2009. Thermal degradation of monoethanolamine at stripper conditions. Energy Procedia 1, 327–333. https://doi.org/10.1016/j.egypro.2009.01.045.

Frimpong, R.A, Nikolic, H., Bahr, D., Kiran, G., Liu, K., 2021. Pilot scale testing of an advanced solvent in a 0.7 MWe post-combustion CO2 capture unit. Int. J. Greenh. Gas Control 106, 103290. https://doi.org/10.1016/j.ijggc.2021.103290.

Gibbins, J., 2023. Amine Stripper Temperature Profile A Key To Optimising Net-Zero Performance In Post-Combustion Carbon Capture Plants | LinkedIn. LinkedIn. https://www.linkedin.com/pulse/amine-stripper-temperature-profile-key-optimising-net-zero-gibbins/ (accessed January 28, 2024).

Gouedard, C., Picq, D., Launay, F., Carrette, P.L., 2012. Amine degradation in CO2 capture. I. A review. Int. J. Greenh. Gas Control 10, 244–270. https://doi.org/10.1016/j.ijggc.2012.06.015.

GOV.UK. UK becomes first major economy to pass net zero emissions law 2019. https://www.gov.uk/government/news/uk-becomes-first-major-economy-to-pass-net-zero-emissions-law (accessed August 25, 2021).

Grubb, M., 2004. Kyoto and the future of international climate change responses: from here to where. Int. Rev. Environ. Strateg. 5, 15–38.

Gruenewald, M., Radnjanski, A., 2016. Gas–liquid contactors in liquid absorbent-based PCC. Absorption-Based Post-Combustion Capture of Carbon Dioxide 341–363. https://doi.org/10.1016/B978-0-08-100514-9.00014-7.

Han, K., Ahn, C.K, Lee, M.S., 2014. Performance of an ammonia-based CO2 capture pilot facility in iron and steel industry. Int. J. Greenh. Gas Control 27, 239–246. https://doi.org/10.1016/j.ijggc.2014.05.014.

Hatcher N., Alvis S., Weiland R. Gas treating simulation – a holistic perspective part 2: carbon capture. Digital Refining 2013.

IEA, 2021. Net Zero by 2050 – Analysis. IEA. https://www.iea.org/reports/net-zero-by-2050 (accessed December 14, 2023).

IEA, 2020a. Energy Technology Perspectives 2020 – Analysis. IEA. https://www.iea.org/reports/energy-technology-perspectives-2020 (accessed December 14, 2023).

IEA, 2020b. Iron and Steel Technology Roadmap – Analysis. IEA. https://www.iea.org/reports/iron-and-steel-technology-roadmap (accessed December 14, 2023).

Intergovernmental Panel On Climate Change (IPCC), 2023. Climate Change 2021 – The Physical Science Basis: Working Group I Contribution to the Sixth Assessment Report of the Intergovernmental Panel on Climate Change, 1st ed. Cambridge University Press. https://doi.org/10.1017/9781009157896.

Jou, F.Y., Otto, F.D, Mather, A.E., 1994. Vapor-liquid equilibrium of carbon dioxide in aqueous mixtures of monoethanolamine and methyldiethanolamine. Ind. Eng. Chem. Res. 33, 2002–2005. https://doi.org/10.1021/ie00032a016.

Karimi, M., Hillestad, M., Svendsen, H.F., 2011. Investigation of intercooling effect in CO2 capture energy consumption. Energy Procedia 4, 1601–1607. https://doi.org/10.1016/j.egypro.2011.02.030.

Kim, I., Hoff, K.A, Hessen, E.T, Haug-Warberg, T., Svendsen, H.F., 2009. Enthalpy of absorption of CO2 with alkanolamine solutions predicted from reaction equilibrium constants. Chem. Eng. Sci. 64, 2027–2038. https://doi.org/10.1016/j.ces.2008.12.037.

Kim, I., Hoff, K.A, Mejdell, T., 2014. Heat of absorption of CO2 with Aqueous solutions of MEA: new experimental data. Energy Procedia 63, 1446–1455. https://doi.org/10.1016/j.egypro.2014.11.154.

Kim, I., Svendsen, H.F., 2007. Heat of absorption of carbon dioxide (CO2) in monoethanolamine (MEA) and 2-(Aminoethyl)ethanolamine (AEEA) solutions. Ind. Eng. Chem. Res. 46, 5803–5809. https://doi.org/10.1021/ie0616489.

Kim, J., Sovacool, B.K, Bazilian, M., Griffiths, S., Junghwan, L., Yang, M., et al., 2022. Decarbonizing the iron and steel industry: a systematic review of sociotechnical systems, technological innovations, and policy options. Energy Res. Soc. Sci. 89, 102565. https://doi.org/10.1016/j.erss.2022.102565.

Knudsen, J.N, Jensen, J.N, Vilhelmsen, P.J., Biede, O., 2009. Experience with CO2 capture from coal flue gas in pilot-scale: testing of different amine solvents. Energy Procedia 1, 783–790. https://doi.org/10.1016/j.egypro.2009.01.104.

Krótki, A., Więcław-Solny, L., Tatarczuk, A., Spietz, T., Chwoła, T., Dobras, S., 2023. A pilot study comparing MEA and AEEA solvents in carbon capture. Int. J. Greenh. Gas Control 126, 103891. https://doi.org/10.1016/j.ijggc.2023.103891.

Kwak, N.S, Lee, J.H, Lee, I.Y, Jang, K.R, Shim, J.G., 2012. A study of the CO2 capture pilot plant by amine absorption. Energy 47, 41–46. https://doi.org/10.1016/j.energy.2012.07.016.

Lan X., Tans P., Thoning K., NOAA global monitoring laboratory. Trends in globally-averaged CO2 determined from NOAA global monitoring laboratory measurements. 2023. 10.15138/9N0H-ZH07.

Le Moullec, Y., Kanniche, M., 2011. Screening of flowsheet modifications for an efficient monoethanolamine (MEA) based post-combustion CO2 capture. Int. J. Greenh. Gas Control 5, 727–740. https://doi.org/10.1016/j.ijggc.2011.03.004.

Le Moullec, Y., Neveux, T., Azki, A.A, Chikukwa, A., Hoff, K.A, 2014. Process modifications for solvent-based post combustion CO2 capture. Energy Procedia 63, 1470–1477. https://doi.org/10.1016/j.egypro.2014.11.156.

Leites, I.L, Sama, D.A, Lior, N., 2003. The theory and practice of energy saving in the chemical industry: some methods for reducing thermodynamic irreversibility in chemical technology processes. Energy 28, 55–97. https://doi.org/10.1016/S0360-5442(02)00107-X.

Lepaumier, H., da Silva, E.F, Einbu, A., Grimstvedt, A., Knudsen, J.N, Zahlsen, K., et al., 2011. Comparison of MEA degradation in pilot-scale with lab-scale experiments. Energy Procedia 4, 1652–1659. https://doi.org/10.1016/j.egypro.2011.02.037.

Li, K., Cousins, A., Yu, H., Feron, P., Tade, M., Luo, W., et al., 2016. Systematic study of aqueous monoethanolamine-based CO2 capture process: model development and process improvement. Energy Sci. Eng. 4, 23–39. https://doi.org/10.1002/ese3.101.

Liu, J., Wang, S., Svendsen, H.F, Idrees, M.U, Kim, I., Chen, C., 2012. Heat of absorption of CO2 in aqueous ammonia, piperazine solutions and their mixtures. Int. J. Greenh. Gas Control 9, 148–159. https://doi.org/10.1016/j.ijggc.2012.03.013.

Mangalapally, H.P, Notz, R., Asprion, N., Sieder, G., Garcia, H., Hasse, H., 2012. Pilot plant study of four new solvents for post combustion carbon dioxide capture by reactive absorption and comparison to MEA. Int. J. Greenh. Gas Control 8, 205–216. https://doi.org/10.1016/j.ijggc.2012.02.014.

McCann, N., Maeder, M., Attalla, M., 2008. Simulation of enthalpy and capacity of CO2 absorption by aqueous amine systems. Ind. Eng. Chem. Res. 47, 2002–2009. https://doi.org/10.1021/ie070619a.

Miyamoto, O., Maas, C., Tsujiuchi, T., Inui, M., Hirata, T., Tanaka, H., et al., 2017. KM CDR ProcessTM project update and the new novel solvent development. Energy Procedia 114, 5616–5623. https://doi.org/10.1016/j.egypro.2017.03.1700.

Moser, P., Wiechers, G., Schmidt, S., Garcia Moretz-Sohn Monteiro, J., Charalambous, C., Garcia, S., et al., 2020. Results of the 18-month test with MEA at the post-combustion capture pilot plant at Niederaussem – new impetus to solvent management, emissions and dynamic behaviour. Int. J. Greenh. Gas Control 95, 102945. https://doi.org/10.1016/j.ijggc.2019.102945.

Mullen, D., Braakhuis, L., Knuutila, H.K, Gibbins, J., Lucquiaud, M., 2024. Monoethanolamine degradation rates in post-combustion CO2 capture plants with the capture of 100% of the added CO2. Ind. Eng. Chem. Res. 63, 13677–13691. https://doi.org/10.1021/acs.iecr.4c01525.

Mun, J.H., Shin, B.J., Kim, S.M., Kyun You, J., Cheol Park, Y., Chun, D.H., et al., 2022. Optimal MEA/DIPA/water blending ratio for minimizing regeneration energy in absorption-based carbon capture process: experimental CO2 solubility and thermodynamic modeling. Chem. Eng. J. 444, 136523. https://doi.org/10.1016/j.cej.2022.136523.

Nakano K., Inada T., Katayama K., Ujisawa Y., Oboso A. Advanced technologies for blast furnace life extension 2020.
Neerup, R., Rasmussen, V.E, Vinjarapu, S.HB., Larsen, A.H, Shi, M., Andersen, C., et al., 2023. Solvent degradation and emissions from a CO2 capture pilot at a waste-to-energy plant. J. Environ. Chem. Eng. 11, 111411. https://doi.org/10.1016/j.jece.2023.111411.
Notz, R., Mangalapally, H.P, Hasse, H., 2012. Post combustion CO2 capture by reactive absorption: pilot plant description and results of systematic studies with MEA. Int. J. Greenh. Gas Control 6, 84–112. https://doi.org/10.1016/j.ijggc.2011.11.004.
Nwaoha, C., Idem, R., Supap, T., Saiwan, C., Tontiwachwuthikul, P., Rongwong, W., et al., 2017. Heat duty, heat of absorption, sensible heat and heat of vaporization of 2–amino–2–Methyl–1–Propanol (AMP), Piperazine (PZ) and Monoethanolamine (MEA) tri–solvent blend for carbon dioxide (CO2) capture. Chem. Eng. Sci. 170, 26–35. https://doi.org/10.1016/j.ces.2017.03.025.
Oexmann, J., Kather, A., 2010. Minimising the regeneration heat duty of post-combustion CO2 capture by wet chemical absorption: the misguided focus on low heat of absorption solvents. Int. J. Greenh. Gas Control 4, 36–43. https://doi.org/10.1016/j.ijggc.2009.09.010.
Oyenekan, B.A, Rochelle, G.T., 2007. Alternative stripper configurations for CO2 capture by aqueous amines. AIChE J. 53, 3144–3154. https://doi.org/10.1002/aic.11316.
Ramírez-Santos, ÁA., Castel, C., Favre, E., 2018. A review of gas separation technologies within emission reduction programs in the iron and steel sector: current application and development perspectives. Sep. Purif. Technol. 194, 425–442. https://doi.org/10.1016/j.seppur.2017.11.063.
Reddy S., Gillmartin J., Francuz V. Integrated compressor/stripper configurations and methods. US Patent: US 20090205946, 2009.
Ren, T., Liu, L., Jing, Y., Dou, M., Wang, J., Chen, X., et al., 2025. Exploring enhanced CO2 separation from blast furnace gas: a multicolumn vacuum swing adsorption approach with process design and experimental assessment. Sep. Purif. Technol. 354, 129300. https://doi.org/10.1016/j.seppur.2024.129300.
Rezazadeh, F., Gale, W.F, Akram, M., Hughes, K.J, Pourkashanian, M., 2016. Performance evaluation and optimisation of post combustion CO2 capture processes for natural gas applications at pilot scale via a verified rate-based model. Int. J. Greenh. Gas Control 53, 243–253. https://doi.org/10.1016/j.ijggc.2016.08.003.
Salih, H.A, Pokhrel, J., Reinalda, D., AlNashf, I., Khaleel, M., Vega, L.F, et al., 2021. Hybrid – slurry/nanofluid systems as alternative to conventional chemical absorption for carbon dioxide capture: a review. Int. J. Greenh. Gas Control 110, 103415. https://doi.org/10.1016/j.ijggc.2021.103415.
Shoeld M. Purification and separation of gaseous mixtures. US Patent: US 1971798A, 1934.
Sultan, H., Quach, T.Q., Muhammad, H.A, Bhatti, U.H, Lee, Y.D, Hong, M.G, et al., 2021. Advanced post combustion CO2 capture process – a systematic approach to minimize thermal energy requirement. Appl. Therm. Eng. 184, 116285. https://doi.org/10.1016/j.applthermaleng.2020.116285.
Suresh Babu A., Rochelle G.T. Heat loss and energy use in pilot plant testing of piperazine with the advanced stripper 2021. 10.2139/ssrn.3811548.
Swalec C. Guest post: these 553 steel plants are responsible for 9% of global CO2 emissions. Carbon Brief 2021. https://www.carbonbrief.org/guest-post-these-553-steel-plants-are-responsible-for-9-of-global-co2-emissions/ (accessed December 14, 2023).
Tatarczuk, A., Tańczyk, M., Więcław-Solny, L., Zdeb, J., 2024. Pilot plant results of amine-based carbon capture with heat integrated stripper. Appl. Energy 367, 123416. https://doi.org/10.1016/j.apenergy.2024.123416.
The Engineering Toolbox. Carbon dioxide - specific heat of gas vs. Temperature 2005. https://www.engineeringtoolbox.com/carbon-dioxide-d_974.html (accessed May 1, 2025).
The University of Sheffield. TERC pilot plant training course: amine capture plant 2024.
The University of Sheffield. Standard operating procedure for amine capture plant (ACP) 2023.
Thimsen, D., Maxson, A., Smith, V., Cents, T., Falk-Pedersen, O., Gorset, O., et al., 2014. Results from MEA testing at the CO2 technology Centre Mongstad. Part I: post-combustion CO2 capture testing methodology. Energy Procedia 63, 5938–5958. https://doi.org/10.1016/j.egypro.2014.11.630.
Thompson, J., Nikolic, H., Combs, M., Bhatnagar, S., Pelgen, J., Abad, K., et al., 2017. Solvent degradation and emissions from a 0.7MWe Pilot CO2 capture system with two-stage stripping. Energy Procedia 114, 1297–1306. https://doi.org/10.1016/j.egypro.2017.03.1242.
Tobiesen, F.A, Svendsen, H.F, Mejdell, T., 2007. Modeling of blast furnace CO2 capture using amine absorbents. Ind. Eng. Chem. Res. 46, 7811–7819. https://doi.org/10.1021/ie061556j.
UNFCCC. Integrating hard-to-abate industries in the process of preparing and implementing NDCs. 2024.
UNFCCC, 1992. United Nations Framework Convention on Climate Change United Nations. United Nations Framework Convention on Climate Change, pp. 1–33.
United Nations (UN). The Paris agreement. 2015.
Vega, F., Sanna, A., Navarrete, B., Maroto-Valer, M.M, Cortés, V.J., 2014. Degradation of amine-based solvents in CO2 capture process by chemical absorption. Greenh. Gases Sci. Technol. 4, 707–733. https://doi.org/10.1002/ghg.1446.
Verma, N., Verma, A., 2009. Amine system problems arising from heat stable salts and solutions to improve system performance. Fuel Process. Technol. 90, 483–489. https://doi.org/10.1016/j.fuproc.2009.02.002.
Vinjarapu, S.HB., Regueira, T., Neerup, R., von Solms, N., Fosbøl, P.L, 2024. Heat of absorption of CO2 in 30 wt% MEA with monoethyleneglycol and urea as vapour reduction additives. Energy 293, 130609. https://doi.org/10.1016/j.energy.2024.130609.
Vogl, V., Olsson, O., Nykvist, B., 2021. Phasing out the blast furnace to meet global climate targets. Joule 5, 2646–2662. https://doi.org/10.1016/j.joule.2021.09.007.
Wanderley, R.R, Pinto, D.DD., Knuutila, H.K., 2020. Investigating opportunities for water-lean solvents in CO2 capture: VLE and heat of absorption in water-lean solvents containing MEA. Sep. Purif. Technol. 231, 115883. https://doi.org/10.1016/j.seppur.2019.115883.
Weiland R., Hatcher N., Alvis S. Pinched performance: part 1. Digital Refining 2015.
Wells, J., Heeley, A., Akram, M., Hughes, K.J, Ingham, D.B, Pourkashanian, M., 2025. Simulation and modelling study of a chemical absorption plant to evaluate capture effectiveness when treating high CO2 content iron and steel industry emissions. Fuel 380, 133189. https://doi.org/10.1016/j.fuel.2024.133189.
Wiley, D.E, Ho, M.T, Bustamante, A., 2011. Assessment of opportunities for CO2 capture at iron and steel mills: an Australian perspective. Energy Procedia 4, 2654–2661. https://doi.org/10.1016/j.egypro.2011.02.165.
Woodhouse S., Rushfeldt P. Absorbent regeneration with flashed lean solution and heat integration. US Patent: US 20100062926, 2010.
World Steel Association. World Steel Short Range Outlook April 2026. 2026.
World Steel Association. World steel in figures 2025. 2025.
Xue, B., Yu, Y., Chen, J., Luo, X., Wang, M., 2017. A comparative study of MEA and DEA for post-combustion CO2 capture with different process configurations. Int. J. Coal Sci. Technol. 4, 15–24. https://doi.org/10.1007/s40789-016-0149-7.
Zhao, Q., Liu, C., Li, P., Zhou, Y., Shen, B., Sun, H., 2026. A critical review on catalytic regeneration of amine solutions for energy-efficient CO2 capture. Carbon Hydrog. 28, 4–20. https://doi.org/10.1002/cbh2.70052.
Zoannou, K.S, Sapsford, D.J, Griffiths, A.J., 2013. Thermal degradation of monoethanolamine and its effect on CO2 capture capacity. Int. J. Greenh. Gas Control 17, 423–430. https://doi.org/10.1016/j.ijggc.2013.05.026.